University of Stavanger

Faculty of Science and Technology

MASTER'S THESIS

Study program/ Specialization: Petroleum technology - Production	Spring semester, 2012 Open
Writer: Eirik Høvring	…… (Writer's signature)
Faculty supervisor: Thor Martin Svartås External supervisor(s): Thor Martin Svartås	
Titel of thesis: **On the activation energy for the formation of a critical size water cluster in structure I and structure II gas hydrates**	
Credits (ECTS): 30	
Key words: Gas hydrate, activation energy, Arrhenius equation, nucleation, growth, cell constant, KHI, PVCap, PVP, cooling rate	Pages: 71 + enclosure: 1 Stavanger, 14/06-2012 Date/year

Acknowledgements.

I would like to express my sincere thanks to my supervisor Dr. Thor Martin Svartås for his continuous supervision and help along the way. Without him, the process of completing this thesis would have become much more difficult.

I would also like to thank Magnus Palm, Sjur Meling Eriksen, Silje Bru and Leif Inge Kjærvoll Sørskår for a nice time together in the laboratory.

Of these people, I would like to express a big thanks to Magnus Palm for all the good discussions we had regarding gas hydrates, and an especially big thanks to Silje Bru and Leif Inge Kjærvoll Sørskår for performing a large amount of experiments for me.

Abstract.

In the present thesis, experiments have been performed in order to study the activation energy for the formation of a stable, critical size water cluster in structure I and structure II gas hydrates. This activation energy represents an energy barrier for the nucleation process forming the required particle (nuclei) size to trigger macroscopic hydrate growth.

The experiments were carried out in different laboratory high pressure cells, but of equal size and geometry. Studies were conducted on two different gases either a system consisting of pure scientific methane (99.9995 % purity) or a seven component natural gas mixture (SNG-7). The aqueous phase was either pure distilled water or distilled water added small amounts of kinetic hydrate inhibitor (KHI). Experimental conditions such as pressure, cooling rate and stirring rate were kept constant for a given experimental series, but different series could be conducted at different conditions. To determine the activation energy a minimum of three experimental temperatures were required at each experimental condition. Experiments were conducted at either 90 bars or 61 bar pressure and at cooling rates ranging from 2 °C/h to 6.75 °C/h. Fluid volumes (water + gas) were kept the same for all experiments (50 and 91.4 ml respectively). Two different KHIs were used; either PVCap with a molecular weight of 6000 Daltons or PVP with a molecular weight of 15000 Daltons. The concentration of KHI was 50 ppm based on the water phase in all experiments.

Arrhenius equation and Arrhenius plots were used to estimate the activation energy of a critical size water cluster. The radius of the critical size water cluster could be determined once the activation energy was known by assuming heterogeneous nucleation and the surface tension between hydrate and water to be 0.0276 J/m^2. Heterogeneous nucleation gives smaller cluster radius than homogeneous nucleation.

In pure systems without KHI present it was concluded that the activation energy mainly was dependent on the type of fluid in the system. An increase of activation energy of approx. 27 % by increasing system pressure from 61 to 90 bar was observed, but the number of pressures examined (2) are too few to make final conclusion on effect of pressure. A slight increase of activation energy by approx. 5 % was observed at 90 bars reducing cooling rate from 6.75 °C/h to 2 °C/h, but the number of cooling rates examined (2) are too few to make final conclusion on effect of cooling.

It was concluded that the experimental cells could have different impact on the measured activation energy, as experiments conducted at similar experimental conditions in Cell #1 and Cell #3 gave not only differences in induction times, but also different activation energies. The latter was assumed due to problems of mechanical character in Cell #1, but this has not been verified by repeating the experiments in one of other, similar cells (Cell #0 or Cell #2, occupied by other students). Apparently Cell #1 required higher driving force for nucleation to occur and behaved more “stochastic” than the other cells. Cell #1 results are thus assumed less reliable than Cell #3 (SNG-7 system) and Cell #2 (pure methane) experiments.

The radius of the critical cluster size for methane sI hydrate was estimated to approx. 39 Å from experiments by this thesis work while Larson and Garside estimated the cluster size to be 32 Å from nucleation theory. Englezos et al. suggested critical size nuclei of the range 30 to 170 Å at the required activation energy for sustainable macroscopic growth. Nerheim et al. proposed approx. 100 Å. The critical size nucleus is larger than the critical size cluster at the energy barrier for the nucleation process.

In Cell #3 PVCap gave an activation energy lower than distilled water baseline. This result is logical because PVCap could act as a promoter on the nucleation process. PVCap may cause water molecules to arrange in a hydrate like structure around the Cap monomer heads. On the other hand, in Cell #1 PVCap gave activation energy higher than distilled water baseline. An explanation for the deviating Cell#1 behavior could be due to mechanical equipment problems or too few experiments performed resulting in overestimated activation energy.

PVP (Cell #3) gave activation energy higher than the distilled water baseline. The explanation for this is that PVP disturbs water structure and acts as an inhibitor on the nucleation phase.

Nomenclature.

T: Temperature

T^{exp}: Experimental temperature

T^{eq}: Equilibrium temperature

P: Pressure

P^{exp}: Experimental pressure

V: Volume

ΔT: Subcooling

ΔS: Entropy

ΔH: Enthalpy

RPM: Rotations per minute

K_n: Equilibrium constants

f: Constant decided by the degree of filling to hydrate lattice at given PT-conditions

h: Constant decided by hydrate lattice

ΔG: Gibbs free energy

ΔG_{crit}: Critical Gibbs free energy (also known as activation energy) for homogenous nucleation

$\Delta G_{crit}'$: Critical Gibbs free energy for heterogeneous nucleation

ΔG_{growth}: Critical Gibbs free energy for a self-sustaining macroscopic growth

ΔG_s: Contribution to Gibbs free energy coming from the structuring at the surface of clusters

ΔG_V: The energy contribution coming from that part of clusters that already has a finished structure

ΔG_v: Change in free energy per unit volume of formed hydrate

Δg^{exp}: Change in total molar Gibbs free energy

υ_h: Molar volume of hydrate

υ_w: Molar volume of water

$f_{b,j}$: Bulk phase experimental fugacity of component j at temperature T

$f_{\infty,j}$: Bulk phase equilibrium fugacity of component j at temperature T

n_w: Number of water molecules per gas molecule

Θ_j: The fractional filling of the hydrate cavities on a free water basis

Θ: The contact angle between the surface and hydrate crystal

φ: Fraction, which if multiplied with ΔG_{crit} gives $\Delta G_{crit}'$

σ: Surface tension between hydrate and water

r: Radius of a water cluster/nucleus

r_{crit}: Radius of a critical size water cluster

r_{growth}: Radius of a critical size nucleus

P_m: The probability of forming m clusters during a time interval Δt

J: The nucleation rate

τ_0: Lag time

t: Induction time

Δt: Time of appearance of a stable cluster

K: Rate of reaction

E_a: Activation energy

k: The Boltzmann constant

R: The gas constant

N_A: Avogadro`s number

A and J_0: The pre-exponential factor

Table of Contents

1. Introduction.

1.1: Gas Hydrates – A general overview.

Gas hydrates are crystalline ice-like solids formed by hydrogen bonded water molecules ("host" molecules) structured around cages in which gas molecules ("guests") are encaged and kept in place by weak van der Waals forces. Whereas the crystal lattice itself is not usually stable, the encaged guest molecules will contribute to stabilize it by shielding repulsive forces between the lattice water molecules. Methane, ethane, propane and carbon dioxide are the most common gas molecules in the natural gas hydrates. Although gas hydrates look like ice, their properties are quite unlike as they can exist at temperatures higher than the ice point and also have structural differences. [1] Four conditions have to be met simultaneously in order for gas hydrates to form:

- Presence of water and gas
- High pressure and low temperature

The process of hydrate formation is exothermal (heat is released). [2]

Gas hydrates are known as nuisance for the petroleum industry with the risk of pipeline plugging causing costly operations. It has therefore become important to develop methods in order to prevent hydrate formation. Methods to avoid gas hydrate formation include:

- Thermodynamic methods (heating, line burial, thermodynamic inhibitor injection)
- Injection of kinetic hydrate inhibitors (KHI)
- Injection of antiagglomerants (AA)
- Cold flow technique [1]
- Removal of free and vaporized water by separation and drying of gas [3]

On the other hand there are vast amounts of natural gas stored in hydrate state in permafrost in Arctic and Antarctic regions and in subsea sediments around the world and those hydrates are considered as a future energy source. The main gas in naturally occurring hydrates is methane which is a more potent greenhouse gas than carbon dioxide. Thus gas hydrates in permafrost and sediments may be a threat to the environment in case of geological events

such as earth quakes resulting in hydrate decomposition and release of huge amounts of methane rich gas to the atmosphere.

THI`s (Thermodynamic Hydrate Inhibitors) prevent the formation of gas hydrates by moving the phase equilibrium curves to lower temperatures and higher pressures. This happens as the inhibitor molecule competes with the water and hydrocarbon molecule (changing the chemical potential of hydration). The most used THI`s are methanol (MeOH) and mono-ethylene glycol (MEG). [4] A drawback with THI`s is that they have to be added in big amounts in order to achieve effective hydrate inhibition (20-50 wt% based on the water phase is normally used). A technology newer than THI`s are low dosage hydrate inhibitors (LDHI`s), which are added in concentrations of approx. 0.1-1.0 wt% based on the water phase to reach the same level of effectiveness as THI`s. [5]

KHI`s (Kinetic Hydrate Inhibitors) are low-molecular-weight polymers and small molecules dissolved in a carrier solvent that are injected into the water phase in pipelines. They bond to the hydrate surface and prevent significant crystal growth for a period longer than the free-water residence time in pipelines. Condensate is not required for this prevention method to be effective.

AA`s (Antiagglomerants) are dispersants that cause the water phase to be suspended as small droplets in the oil or condensate. When the suspended water droplets convert to hydrates, pipeline flows are maintained without blockage. Because AA`s relies on emulsified water/hydrates, a condensed hydrocarbon is required. [6]

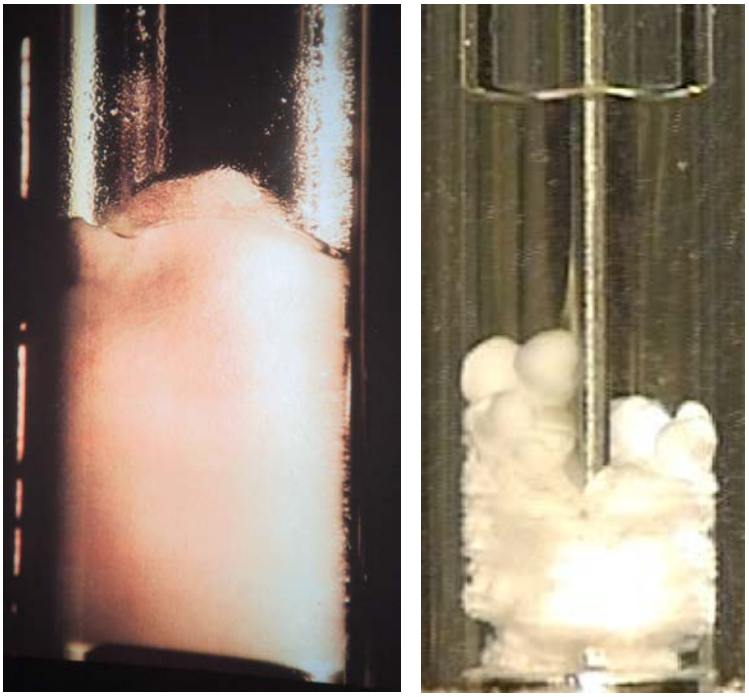

- **Figure 1.1.1: Gas hydrate formed from water and the seven component gas mixture (SNG-7) used in most experiments in the present thesis. The figure on the left shows SNG-7 hydrate in sapphire cell and right figure hydrate spheres formed under influence of a chemical inhibitor [7]**

Gas hydrates served only as a curiosity before the scientist Hammerschmidt in 1934 identified hydrate formation in pipelines that ran through cold areas, effectively blocking the production of oil and gas. [8] Gas hydrates have become an important research area ever since this discovery, with the main focus being on the prevention and removal of hydrate plugs in pipelines for the transportation of oil and gas.

Formation of gas hydrates in pipelines can cause a delay of production, which in itself can be very costly due to lost production time. A cost also lies in the removal of hydrates as this is both a time consuming and comprehensive process. An example on this is a hydrate blockage that occurred in the export line from Shell`s Bullwinkle platform in the Green Canyon Block 65. The 12 inch, 39000 ft line was not insulated. The temperature in the seawater was 50 ^{o}F at the base of the platform in 1400 ft of water. The flowrate was 140 MMscf/d at an inlet pressure of 800 psi, and the gas gravity was 0.7. The platform was shut down due to a hurricane, and during restart gas hydrates started to form. The gas dehydrator was partially filled with water during the shut-in period. Because the gas dehydrator was not cleaned properly when the production restarted, it did not dehydrate gas as designed and wet gas entered the export line, causing water condensation and hydrate formation. This resulted in a

complete hydrate blockage in no less than 1 hour, just past the base of the export riser at a low spot. The line was depressurized on both sides of the plug in order remove the hydrate. After this, methanol was circulated into the line to accelerate the hydrate dissociation rate. After complete removal of the hydrate, the dehydrator was cleaned, inspected and restarted properly. This entire operation of remedial took 36 hours to complete. In this case, the major cost was lost production time.

Hydrates can also cause damage to equipment as shown in the figure below: [3]

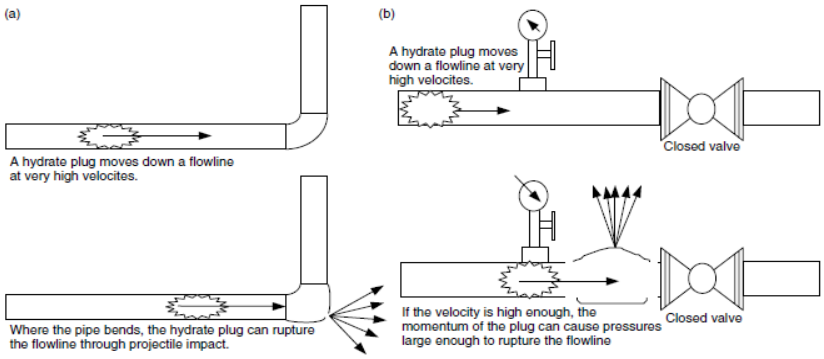

- **Figure 1.1.2: A hydrate plug moving at high velocity in a pipeline. a) The plug acts as a projectile, rupturing the pipeline at the bend. b) The plug cause pressures large enough in front of the closed valve to rupture the pipeline [3]**

In addition, hydrates may pose a risk to life. Cases of major injuries and major damage to equipment due to hydrates are reported every few years. [9] For instance, a hydrate plug incident that resulted in loss of life occurred at a major energy company in Alberta. A foreman and an operator were trying to remove a hydrate plug in an outlying sour gas flowline. They had bled down the pressure in the distant end from the wellhead, and were standing near the pipeline when the line failed due to an impact caused by a hydrate mass acting as a projectile at very high velocity. A big piece of pipe struck the foreman and the operator called for help. The foreman was declared dead on arrival at the hospital.

Gas hydrate formation is one of the most important problems related to flow assurance. Asphaltenes, scale, waxes and corrosion are considered lesser problems. As an example, gas hydrates are considered the largest problem compared to any other in the Gulf of Mexico. [3]

Hydrate plugs in pipelines occur during transient and abnormal operations such as:

- When uninhibited water is present due to dehydrator failure or inhibitor injection failure
- When cooling occurs with flow across a valve or restriction
- Start-up
- Operational shut-in
- Restart following an emergency

The formation of a hydrate plug does not occur during normal flowline operation, or in the absence of unforeseen failures. Most oil production pipelines are insulated by design to maintain the temperature as high as possible in the flowstream before arrival at the platform, in order to avoid the hydrate formation region. Oil dominated systems typically has a higher heat capacity to maintain the reservoir temperature than systems dominated by gas, which allows the system to be less prone to the formation of gas hydrates. On the other hand, systems dominated by gas cool down more quickly compared to oil-dominated systems. This requires gas-dominated systems to be inhibited, in order to avoid the formation of hydrates.

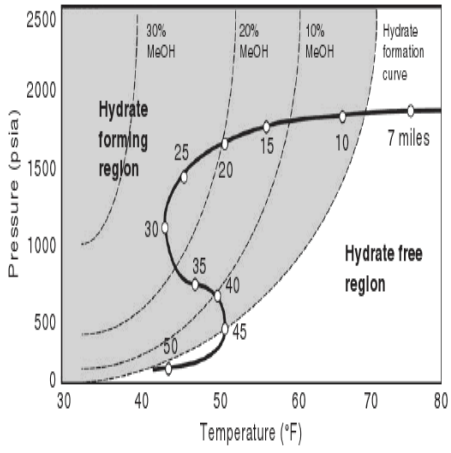

- **Figure 1.1.3: Hydrate formation pressures and temperatures (the gray part) as a function of methanol concentration for a given gas mixture in free water. Steady-state flowline fluid conditions are shown at distances (indicated as 7-50 miles on the curve) along the bold black curve [10]**

Figure 1.1.3 serves as an example on transportation of hydrocarbons from a subsea wellhead. When at 7 miles away from the subsea wellhead, the steady-state flowing stream retains some reservoir heat, meaning there is no possibility of hydrate formation. The ocean cools down the

flowing stream and at about 9 miles a unit mass of gas and associated water enters the hydrate region to the left of the hydrate formation curve, remaining in the uninhibited hydrate area until mile 45. By mile 30, the temperature of the pipeline system is a few degrees higher than the deep ocean temperature, so that approximately 23 wt% methanol is required in the free water phase to shift the hydrate formation region to the left of flowline conditions to prevent hydrate formation and blockage.

Formation of hydrate and accumulation occurs in the free water phase. Usually just downstream of water accumulations, where there is a change in flow geometry (for example a bend or pipeline dip along a depression in the ocean floor). It can also occur at sites of nucleation (for example sand). The figure below shows several places where hydrate can form in an offshore system. [10]

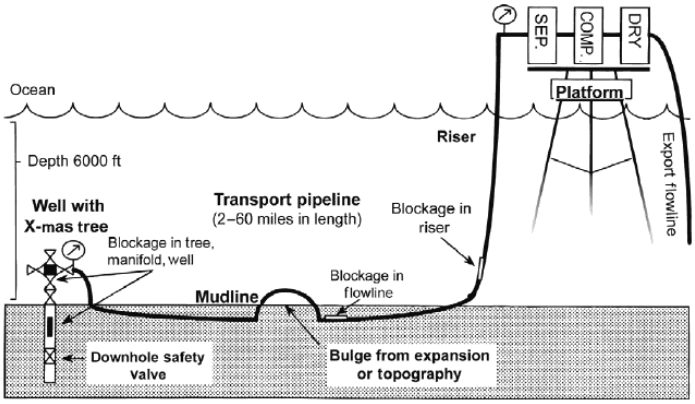

- **Figure 1.1.4: Schematic of an offshore system. The points show where hydrate formation might occur in a pipeline for transportation of hydrocarbons [10]**

The first response usually made when hydrate plugs a pipeline for transportation of hydrocarbons is to locate the plug and determine its position and length. After this, it is common to evaluate the safety concerns of plug removal and then evaluate and decide which method of plug removal should be used. The hydrate plug removal methods include:

- Hydraulic methods: Depressurization
- Chemical methods: Injection of inhibitors or reactive chemicals that generate heat, etc.
- Thermal methods: Direct electrical heating
- Mechanical methods: Use of coiled tubing or drilling

The preferred method of hydrate plug removal from a safety and technical point of view is to depressurize the plug from both sides. For that reason, depressurization will be the only method of removal discussed in this section. This method is particularly complicated to use when the liquid head on the hydrate plug is greater than the dissociation pressure, as is the case in very deep water. In such a case, electrical heating may be implemented to dissolve the hydrate. [3]

By reducing the pressure, the hydrate is no longer in a stable phase. It should be noted that depressurization has little effect on the freezing point of ice. However, in theory, this method should also work effectively for ice.

The best way to perform depressurization of a hydrate plug is to try and maintain the pressure nearly equal on both sides of the plug. This results in the prevention of any significant movement of the plug, thus avoiding any danger of a fast moving projectile in the pipeline. If it is not possible to bleed off the pressure from both sides of the plug, the alternative is to bleed off pressure from only one of the sides. A huge problem with this method is that much pressure must be bled off in order to melt the hydrate plug, but not so much bleeding off is required for the plug to become a projectile. If the pressure in the pipeline is above the hydrate formation pressure, then bleeding off some pressure will not melt the hydrate. If the pipeline pressure is high, even bleeding off 1400-2000 kPa, which is sufficient to create a projectile, may not be enough to melt the hydrate. [11]

Pipeline depressurization reduces the hydrate temperature below the temperature of the surroundings. The heat transport from the surroundings flow radially into the pipe and causes dissociation of the hydrate plug to commence at the pipe wall. This is shown in figure 1.1.5. Radial dissociation is not always the case, as the dissociation also can start at the ends of the plug. [3]

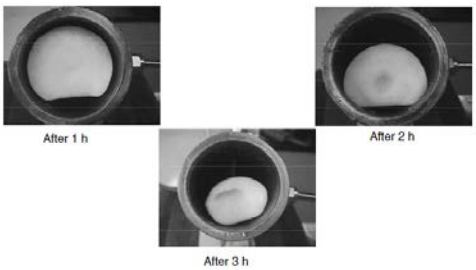

- **Figure 1.1.5: Hydrate plug radial dissociation [3]**

1.2: Definition of the thesis.

In previous studies on the activation energy for hydrate formation, the focus has been on the activation energy at the point of macroscopic growth where hydrates start to grow self-sustainingly. This process is normally studied in constant pressure system measuring the amount of gas added per unit time to maintain constant pressure (as in [12-14]). There are no records of studies in literature which deals with the activation energy related to the formation of a critical size water cluster at the energy barrier of nucleation. This critical size water cluster is the precursor for the formation of critical size nuclei for the macroscopic growth process to proceed self-sustainingly. A certain amount of energy is required to form the critical size water cluster: An activation energy corresponding to the energy barrier for the nucleation process to commence.

There are still many factors that remain unknown regarding the hydrate nucleation process. It is therefore of great interest to study the activation energy or the energy barrier related to the formation of a stable critical sized water cluster, as this serves as an untouched research area. The interaction between kinetic hydrate inhibitors (KHI) and the energy barrier and nucleation rates may be of great importance for the development of better hydrate inhibitors.

The objective of this MSc thesis has thus been to study the activation energy at the energy barrier for the formation of critical size water cluster at the commencement of the hydrate nucleation process. A huge amount of experimental measurements were included in the analysis, in order to achieve an improved understanding of this process.

2. Theory.

2.1: The cavities in hydrates.

The three hydrate structures (sI, sII and sH) are built up of five polyhedral, formed by hydrogen-bonded water molecules. They are shown in figure 2.1.1, and additional cavity information is given in table 2.1.1. The nomenclature description for these polyhedral is n_i^{mi}. For a face type "i", n_i is the number of edges found in this face type and m_i is the number of faces with n_i edges. [15]

The pentagonal dodecahedron ($n_i^{mi} = 5^{12}$), is a 12-sided cavity, present as the small cavity in all the known natural gas hydrate structures. It has 12 pentagonal faces with equal edge lengths and equal angles.

The tetrakaidecahedron ($n_i^{mi} = 5^{12}6^2$), is a 14-sided cavity, present as the large cavity in structure I (sI) hydrate. It has 12 pentagonal and 2 hexagonal faces.

The hexakaidecahedron ($n_i^{mi} = 5^{12}6^4$), is a 16-hedron, present as the large cavity in structure II (sII) hydrate. It has 2 more hexagonal faces than the $5^{12}6^2$ cavity found in sI hydrate.

The irregular dodecahedron ($n_i^{mi} = 4^35^66^3$), has 3 square faces, 6 pentagonal faces and 3 hexagonal faces. It is found as the medium sized cavity in structure H (sH) hydrate. Hydrate structures I and II have 2 cavity types, while sH has 3 cavity types (small: 5^{12}, medium: $4^35^66^3$) where the third and largest cavity is the icosahedron ($n_i^{mi} = 5^{12}6^8$). It has 12 pentagonal faces, 6 hexagonal faces and a hexagonal face each at the cavity crown and foot.

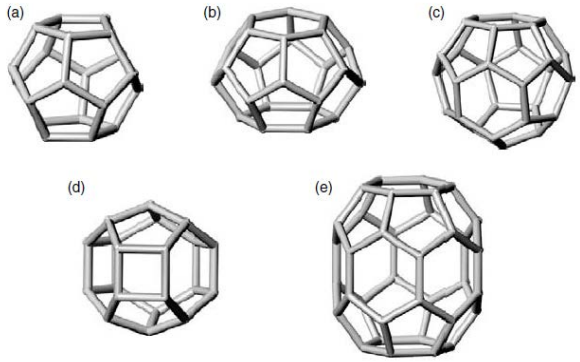

- **Figure 2.1.1: The five polyhedra of the hydrate structures. a) Pentagonal dodecahedron (5^{12}), b) Tetrakaidecahedron ($5^{12}6^2$), c) Hexakaidecahedron ($5^{12}6^4$), d) Irregular dodecahedron ($4^35^66^3$), and e) Icosahedron ($5^{12}6^8$) [16]**

The hydrate cavities are expanded relative to ice, and are prevented from collapsing by repulsion of the guest molecules.

All hydrate cavities (except cavities containing square faces) obey Euler`s theorem for convex polyhedral. [16] Euler`s theorem: [17]

$$F + V = E + 2 \qquad (2.1.1)$$

The sum of the number of faces (F) and vertices (V) is the same as the number of edges plus 2. This theorem is fulfilled in cavities having 12 pentagonal faces and any number of hexagonal faces (except 1). As an example, the 5^{12} cavity has 12 faces, 20 vertices and 30 edges. F + V = E + 2 => 12 + 20 = 30 + 2 => LHS = RHS. Euler`s theorem is fulfilled. [16]

- **Table 2.1.1: Cavity geometries, showing in which hydrate structure the different cavity-types acts (reproduced table) [16]**

	Structure I		Structure II		Structure H		
Cavity	**Small**	**Large**	**Small**	**Large**	**Small**	**Medium**	**Large**
Description	5^{12}	$5^{12}6^2$	5^{12}	$5^{12}6^4$	5^{12}	$4^3 5^6 6^3$	$5^{12}6^8$
Number of cavities/unit cell	2	6	16	8	3	2	1
Average cavity radius [Å]	3,95	4,33	3,91	4,73	3,94	4,04	5,79
Variation in radius [%]	3,4	14,4	5,5	1,73	4	8,5	15,1
Number of water molecules/cavity	20	24	20	28	20	20	36

2.2: Hydrate crystal structures.

Hydrates are classified with respect to the water molecule arrangement in the crystals.
Three crystal structures exist that are made up from components of natural gas:

- Structure I (sI)
- Structure II (sII)
- Structure H (sH)

Over 130 compounds that form hydrates with water molecules usually form sI, sII or sH. Emphasis is given to sI and sII, since they are the most common natural gas hydrate structures to occur in the petroleum industry. Structure H can also occur in the petroleum industry, but this is not common.
Other structures also exist, as Jeffrey (in 1984) listed seven hydrate structures (I-VII). Of these structures only structure I and II have been shown to contain hydrocarbon gas components. Also, structure H is absent from this list. For more information on Jeffrey`s list, see reference [16].
Below, detailed information is given about the natural gas hydrate structures: [16]

Structure I (sI): The least complex hydrate structure. It is built up of two polyhedral cavity types, one small and one large. The small cavity is a dodecahedron, while the large cavity is a tetrakaidecahedron.
There are 46 water molecules per unit cell for sI hydrate, and a unit cell consists of 2 small and 6 large cavitites.
The most common sI formers are methane (CH_4), ethane (C_2H_6), carbon dioxide (CO_2) and hydrogen sulfide (H_2S). The size of the cavities determines the type of gas molecules that can fit into them. Molecules with sizes in the range 4.4 – 5.4 Å, including the above mentioned sI formers (excluding ethane), are able to fit into both the small and large cavities of sI. Still larger molecules ranging from 5.6 -5.8 Å, including sI former ethane, are too large to fit into the small cavities and can only fit into the large cavities.

Structure II (sII): Hydrate structure II is more complex compared to structure I. Similar to sI, sII is also built up of two hydrate cavities. The small cavity is a dodecahedron, while the large cavity is a hexakaidecahedron.

Structure II unit cells consist of 136 water molecules, and for each unit cell there are 16 small and 8 large cavities.

Common sII formers in natural gas are nitrogen (N_2), propane (C_3H_8) and isobutane (i-C_4H_{10}). Nitrogen can occupy both the small and large cavities of sII. Propane and isobutane can only occupy the large cavities.

Sizes of propane and isobutane lie in the range of 6.0 – 6.9 Å. Molecules larger than 7 Å, are too big to form either sI or sII.

Structure H (sH): This is the hydrate structure that occur the least compared to sI and sII. Hydrate structures I and II can form in the presence of only one hydrate former, while sH requires a small guest molecule (as methane) and a structure H former. This type of hydrate is built up of three cavities. The small cavity is a dodecahedron, the medium sized cavity is an irregular dodecahedron and the large cavity is an irregular icosahedral.

Structure H unit cells consist of 34 water molecules, and for each unit cell there are 3 small cavities, 2 medium sized cavities and 1 large cavity.

Natural gas molecules that form sH hydrate are 2-methylbutane, 2.2-dimethylbutane, 2.3-dimethylbutane, 2.2.3-trimethylbutane, 2.2-dimethylpentane, 3.3-dimethylpentane, methylcyclopentane, ethylcyclopentane, methylcyclohexane, cycloheptane, and cyclooctane. These molecules are not usually found in natural gas, explaining why sH is less common than sI and sII. [18]

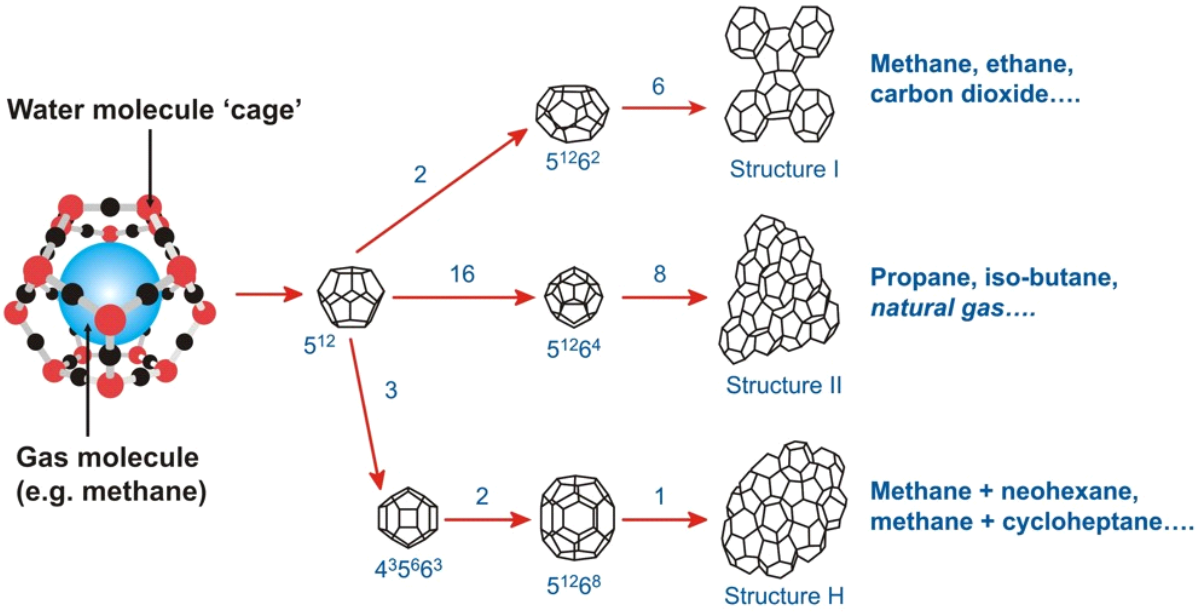

- **Figure 2.2.1: Hydrate cavities and hydrate structures I, II and H [19]**

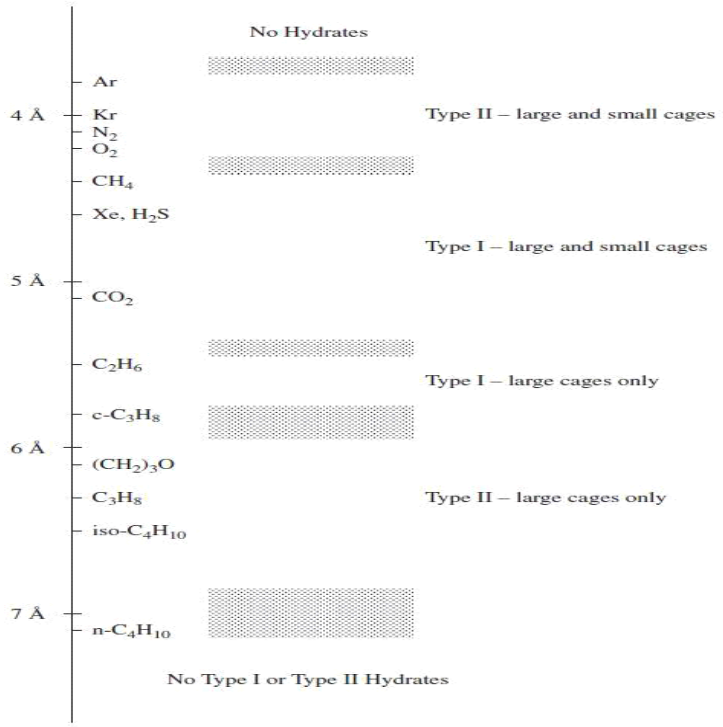

- **Figure 2.2.2: Size of guest molecules, occupied cavities and hydrate structures [18]**

- **Table 2.2.1: Comparison of structure I and structure II hydrates (reproduced table) [18]**

	Structure I	**Structure II**
Water molecules per unit cell	46	136
Cavities per unit cell		
Small	2	16
Large	6	8
Theoretical formula		
All cages filled	$X*5^3/_4H_2O$	$X*5^2/_3H_2O$
Mole fraction hydrate former	0,1481	0,1500
Only large cages filled	$X*7^2/_3H_2O$	$X*17H_2O$
Mole fraction hydrate former	0,1154	0,0556
Cavity diameter [Å]		
Small	7,9	7,8
Large	8,6	9,5
Volume of unit cell [m^3]	$1,728*10^{-27}$	$5,178*10^{-27}$
Typical formers	CH_4, C_2H_6, H_2S, CO_2	C_3H_8, i-C_4H_{10}, N_2
Note: X is the hydrate former		

2.3: Mechanistic model for hydrate formation without inhibitor.

A reaction model published by Lekvam and Ruoff describes the separate steps of hydrate formation and growth for a mixture of methane (CH_4) and distilled water. Both the induction time and the step for macroscopic crystal growth are included in the model. The model consists of five pseudo elementary steps:

$$CH_4(g) \underset{K_{-1}}{\overset{K_1}{\rightleftarrows}} CH_4(aq) \qquad (2.3.1)$$

Methane in gas phase (g) is dissolved into the water phase (aq) during stirring.

$$f.CH_4(aq) + h * H_2O \underset{K_{-2}}{\overset{K_2}{\rightleftarrows}} N \qquad (2.3.2)$$

The clusters (N) that are formed have not yet reached critical size, and are therefore not thermodynamically stable. Until critical size is reached, the clusters will continue to form and dissolve.

$$N \overset{K_3}{\rightarrow} H \qquad (2.3.3)$$

A cluster has reached critical size. It is now thermodynamically stable and can through spontaneous growth form a hydrate (H). Equation (2.3.3) is driven towards right.

$$N \underset{K_{-4}}{\overset{K_4\,[H]}{\rightleftarrows}} H \qquad (2.3.4)$$

N in equation (2.3.4) could be the secondary cluster formed from hydrate crystals that have been fragmented into pieces because of mechanical impact from the stirring mechanism. It can therefore be assumed that there are both secondary nucleation and hydrate in the system.

$$f.CH_4(aq) + h * H_2O \underset{K_{-5}}{\overset{K_5[H]}{\rightleftarrows}} H \qquad (2.3.5)$$

Equation (2.3.5) describes what happens at the surface of the already formed hydrate crystals. The hydrate crystal grows by addition of gas and water to the hydrate surface, the water creates new cavities and gas penetrates into the cavities before they close.

In equation (2.3.4) and (2.3.5) the equilibrium constants K_4 and K_5 are multiplied by the concentration of hydrate [H] in the system. This is an indication of the model assuming proportionality between concentration [H] and the free surface area of the hydrate crystals. As the hydrate grows (higher concentration of [H]) the surface area which water can attach to increases in size, which results in an increased velocity of growth. One can then assume that the growth velocity is decided by the surface area. [20]

2.4: Modified mechanistic model for hydrate formation without inhibitor.

Thor M. Svartås and Lindy A. Dybvik modified the reaction model presented by Lekvam and Ruoff in 1993, to include a multicomponent gas mixture in addition to an oil phase. The model was built with basis on a 7-component synthetic natural gas (SNG-7), consisting of 7 hydrate formers, HF_n (n=7, HF_n=C_1, C_2, C_3, i-C_4, n-C_4, N_2 and CO_2). In a gas mixture, each gas component has its own set of rate constants ($k_{\pm Mn}$) and factors of filling (f_n) and the hydrate number, h, is decided by the hydrate structure and size of the hydrate formers present in the gas mixture. The modified model for hydrate formation without inhibitor consists of 6 pseudo elementary steps:

$$G(g) \underset{K`_{-1}}{\overset{K`_1}{\rightleftarrows}} G(l) \qquad (2.4.1)$$

$$G(l) \underset{K`_{-2}}{\overset{K`_2}{\rightleftarrows}} G(aq) \qquad (2.4.2)$$

$$f.G(aq) + \ h * H_2O \underset{K`_{-3}}{\overset{K`_3}{\rightleftarrows}} N \qquad (2.4.3)$$

$$N \overset{K`_4}{\rightarrow} H_1 \qquad (2.4.4)$$

$$N \underset{K`_{-5}}{\overset{K`_5\,[H]}{\rightleftarrows}} H2 \qquad (2.4.5)$$

$$f.G(aq) + \ h * H_2O \underset{K`_{-6}}{\overset{K`_6[H]}{\rightleftarrows}} H_2 \qquad (2.4.6)$$

In these steps we have:

$$\sum_{n=1}^{m} HF_n(g) = G(g), \sum_{n=1}^{m} HF_n(l) = G(l), og \ \sum_{n=1}^{m} HF_n(aq) = G(aq) \qquad (2.4.7)$$

Factor of filling, f, is given as:

$$f = \frac{(S_c \sum_{n=1}^{m} x_{nS} + L_c \sum_{n=1}^{m} x_{nL})}{(S_c + L_c)} \qquad (2.4.8)$$

Where x_{nS} and x_{nL} are molar fractions of component HF_n in the small and large cavities, S_c and L_c are the numbers of small and large cavities in a unit cell of the hydrate structure respectively. All steps are similar to the reaction model presented by Lekvam and Ruoff, with the exception of step (2.4.1) and (2.4.2) where gas is dissolved into the liquid oil phase and gas is dissolved into the water phase respectively. [21]

2.5: Modified mechanistic model for hydrate formation with inhibitor.

The modified model from 1993 did not include reactions between kinetic inhibitors (KHI`s), water molecules and hydrate crystals. This has been implemented in the newer version of the model which is described below. Kinetic inhibitors can mix with water and bind to a number of water molecules, resulting in the clusters (N) being blocked and/or reduced. KHI`s also absorbs to the surface of the micro crystals that are created when hydrate crystals form from clusters, blocking active growth. This has an impact on the time it takes to produce a critical hydrate concentration [H]. Based on the above, this model consists of 8 pseudo elementary steps:

$$G(g) \underset{K`_{-1}}{\overset{K`_1}{\rightleftarrows}} G(l) \qquad (2.5.1)$$

$$G(l) \underset{K`_{-2}}{\overset{K`_2}{\rightleftarrows}} G(aq) \qquad (2.5.2)$$

$$Ki + h * H_2O \overset{K`_3}{\rightarrow} Ki - W \qquad (2.5.3)$$

In equation (2.5.3), Ki-W is a kinetic inhibitor-water complex where n water molecules attach onto inhibitor molecules.

$$fG(aq) + h * h_2O \underset{K`_{-4}}{\overset{K`_4}{\rightleftarrows}} \mathrm{N} \qquad (2.5.4)$$

$$N \overset{K`_5}{\rightarrow} H \qquad (2.5.5)$$

$$H + Ki - W \underset{K`_{-6}}{\overset{K`_6}{\rightleftarrows}} H - Ki - W + m\,H_2O \qquad (2.5.6)$$

H-Ki-W in equation (2.5.6) is a hydrate-kinetic inhibitor-water complex.

$$N \underset{\overleftarrow{K_{-7}}}{\overset{\overrightarrow{K_7[H]}}{\longrightarrow}} H \qquad (2.5.7)$$

$$fG(aq) + h * H_2O \underset{\overleftarrow{K_{-8}}}{\overset{\overrightarrow{K_8[H]}}{\longrightarrow}} \mathrm{H} \qquad (2.5.8)$$

The first 2 steps in the model, (2.5.1) and (2.5.2), are identical to steps (2.4.1) and (2.4.2) from the version without inhibitor. In this revised model, it is assumed that each molecule from the KHI can be associated with a number, n, of water molecules which form a "kinetic inhibitor-water complex", Ki-W. When the clusters, N, reaches critical size, they become stable and transformed into hydrate crystals. This is shown in equation (2.5.5).

The formation of the first stable hydrate crystal from this process is referred to as the start of hydrate growth. The crystal growth continues by addition of water and gas to the surface of the hydrate crystals.

When a KHI is present, a portion of the water will attach to the inhibitor, and it is assumed that the kinetic inhibitor-water complex, Ki-W, can take part in the growth process by forming a hydrate-kinetic inhibitor-water complex, H-Ki-W in step (2.5.6). The formation of a H-Ki-W complex increases the time it takes to produce an active hydrate concentration that exceeds the critical concentration, [H], which trigger steps (2.5.7) and (2.5.8) that ends up in a rapid exothermic reaction. [22]

2.6: Nucleation and induction time.

The process of hydrate formation can be divided into 2 phases: Nucleation and crystal growth. Nucleation is the process in which microscopic clusters of water and gas grow and disperse in an attempt to reach critical size where spontaneous growth occurs. Nucleation is a microscopic phenomenon. It involves a large number of molecules, and is hard to observe experimentally.

Nucleation occurs either free of impurities (homogenous nucleation), or in the presence of impurities (heterogeneous nucleation).

Homogenous nucleation (HON) is very hard to achieve due to the difficulty of obtaining solutions completely free of foreign particles. [23] It can however be achieved by having an oil emulsion with significantly small droplets (ultrapure water) dispersed within it, or forming the droplets by expansion through a supersonic nozzle. [24] Even though homogenous nucleation is a rare event, the classical nucleation theory (origin: Volmer and Weber, 1926) still acts as the basis for the majority of today's works on nucleation. [25] Below is a description of the theory.

The nucleation process consists of a large number of molecules, and the probability for them to collide simultaneously is infinitely small. It is therefore more reasonable to assume that a sequence of bimolecular collisions of an autocatalytic nature occurs. There is a sequential formation of clusters in the supercooled liquid that increases in size, until a critical size water cluster is obtained. The figure below illustrates this phenomenon.

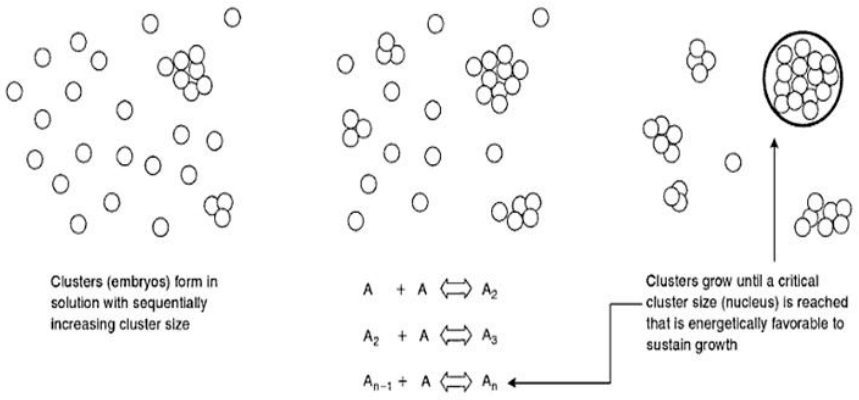

- **Figure 2.6.1: Clusters of water and gas form and disperse in an attempt to reach critical size. Upon reaching the point of critical cluster size, the energy barrier for further growth is breached and spontaneous growth occurs [23]**

The point where the clusters reach critical size can be explained by the increasing Gibbs free energy during their growth, ΔG. As the clusters grow, the Gibbs free energy gradually increases. When a maximum ΔG (activation energy) is reached, the cluster will become energetically favorable to sustain a growth. Maximum Gibbs free energy is given the nomenclature, ΔG_{crit}. It is a function of the surface tension σ which is found in the contact area between the cluster and liquid, and also a function of the radius of the cluster when at critical size r_{crit}. Formula for ΔG_{crit} is given as: [23]

$$\Delta G_{crit} = \frac{4\pi\sigma {r_{crit}}^2}{3} \qquad (2.6.1)$$

The Gibbs free energy for a constant temperature can be expressed as: [26]

$$\Delta G = \Delta H - T\Delta S \qquad (2.6.2)$$

When the clusters start to grow a negative entropy ΔS exists, because of the energy needed to structure/arrange the water molecules in a given pattern (lattice structure) on the surface of the cluster, meaning that the system is in disorder in the beginning. If the clusters are going to continue to grow and become energetically favorable to sustain a growth, the water molecules must first arrange themselves in a certain lattice structure. The contribution of entropy lies in the structuring at the surface of the clusters and is defined by ΔG_s, which is a function of the cluster radius and the surface tension in the contact area/interface between the clusters and liquid. ΔG_s is given by:

$$\Delta G_s = 4\pi r^2\sigma \qquad (2.6.3)$$

Here, r is the cluster radius and σ is the surface tension. ΔG_s is equivalent to TΔS in equation (2.6.2).

The enthalpy, ΔH, is equivalent to ΔG_v which is related to the volume of clusters. ΔG_v represents the energy in that part of the cluster that already has a finished structure and is given by:

$$\Delta G_v = \frac{4}{3}\pi r^3 \Delta g_v \qquad (2.6.4)$$

Where Δg_v = change in free energy per unit volume of formed hydrate, and r = cluster radius (volume of a sphere, $V = 4/3\pi r^3$, if we assume a spherical cluster).
One can now write:

$$\Delta G = \Delta G_s + \Delta G_v = 4\pi r^2\sigma + \frac{4}{3}\pi r^3 \Delta g_v \qquad (2.6.5)$$

Referring to figure 2.6.2, the curve for ΔG will have a turning point at $r = r_{crit}$. At this point, the derived of ΔG with respect to r ($\delta(\Delta G)/\delta r$) equals zero. This makes the right hand side of equation (2.6.5) into:

$$8\pi r\sigma + 4\pi r^2 \Delta g_v = 0 \rightarrow \Delta g_v = -\frac{2\sigma}{r_{crit}} \qquad (2.6.6)$$

Inserting equation (2.6.6) into equation (2.6.5), setting $r = r_{crit}$, leads to:

$$\Delta G_{crit} = 4\pi\sigma {r_{crit}}^2 + \frac{4}{3}\pi {r_{crit}}^3 \left(-\frac{2\sigma}{r_{crit}}\right)$$

$$\Delta G_{crit} = \frac{12}{3}\pi\sigma {r_{crit}}^2 - \frac{8}{3}\pi\sigma {r_{crit}}^2 = \frac{4}{3}\pi\sigma {r_{crit}}^2 \qquad (2.6.7)$$

In the beginning of the growth phase, the clusters will receive a greater contribution of Gibbs free energy from the surface area than from the volume as the area of small particles is relatively large compared to their volume. As the clusters grow, the contribution from volume will increase and become greater than the contribution from the surface area in equation (2.6.3). [23]

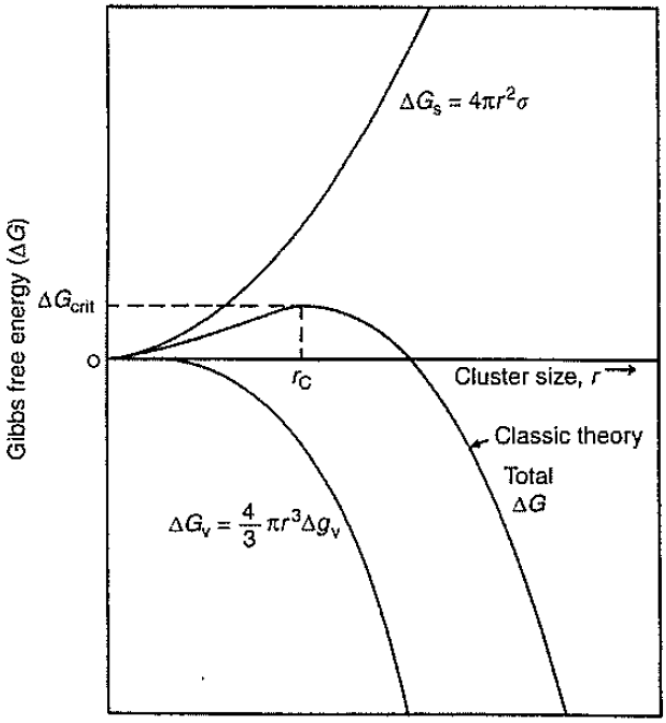

- **Figure 2.6.2: Surface excess free energy (ΔG_s), volume excess free energy (ΔG_V) and total excess free energy (ΔG) as a function of cluster size r [23]**

As an example on the use of this theory, Englezos et al. determined the radius of the critical size nucleus for methane hydrate to be between 30-170 Å assuming spherical shape and using modifications of equations (2.6.6) and (2.6.7). The modifications of these equations are shown below:

$$r_{crit} = -\frac{2\sigma}{\Delta g_v} \qquad (2.6.8)$$

$$(-\Delta g_v) = \frac{RT}{\upsilon_h}\left[\sum_1^2 \theta_j ln\left(\frac{f_{b,j}}{f_{\infty,j}}\right) + \frac{n_w \upsilon_w (P-P_\infty)}{RT}\right] \qquad (2.6.9)$$

Where υ_h and υ_w are the molar volumes of hydrate and water respectively, σ is the surface tension between ice and water, Θ_j is the fractional filling of the hydrate cavities on a basis of free water, $f_{b,j}$ and $f_{\infty,j}$ are the bulk phase experimental and equilibrium fugacities respectively of component j at temperature T, n_w represents the number of water molecules per gas molecule, and (P-P_∞) is the overpressure.

Nerheim et al. determined the radius of the critical size nucleus for methane to be approx. 100 Å by use of laser scattering [27]. This result is in agreement with the size range calculated by Englezos et al.

Larson and Garside estimated the radius of the critical size water cluster for methane sI hydrate to be 32 Å [28].

Heterogeneous nucleation (HEN) is a more common event compared to homogenous nucleation, and it occurs in the presence of impurities (for example particles of dust) or a surface (for example on the interface between liquid and gas, or on the cell wall). HEN occurs at supercoolings lower than what is needed for homogenous nucleation. Looking at it from the perspective of free energy, the probability of forming a cluster on a 2-dimensional surface (a cell wall for example) is greater than the probability of forming a cluster in a 3-dimensional volume of water (free of existing surface). [23] The same thermodynamics and kinetics applies to heterogeneous nucleation as for HON, the difference being in the surface energy term and the geometric relations. [29] The contact angle (Θ) between the surface and hydrate crystal is related to a fraction (φ), which if multiplied with the value of Gibbs free energy for the HON case gives us the value of Gibbs free energy for HEN. This relation is shown below:

$$\Delta G_{crit}{}' = \varphi \Delta G_{crit} \qquad (2.6.10)$$

Where φ as a function of Θ is:

$$\varphi = \frac{[(2+cos\theta)(1-cos\theta)^2]}{4} \qquad (2.6.11)$$

As φ is a fraction, the Gibbs free energy required for spontaneous growth is lower in HEN than in homogenous nucleation. This is because the unknown surface lowers the critical Gibbs free energy. Examples of Gibbs free energy varying with contact angle: [23]

- $\Theta = 180^o$: complete nonwetting of the substrate, $\Delta G_{crit}{}' = \Delta G_{crit}$
- $\Theta = 0^o$: complete wetting of the substrate, $\Delta G_{crit}{}' = 0$

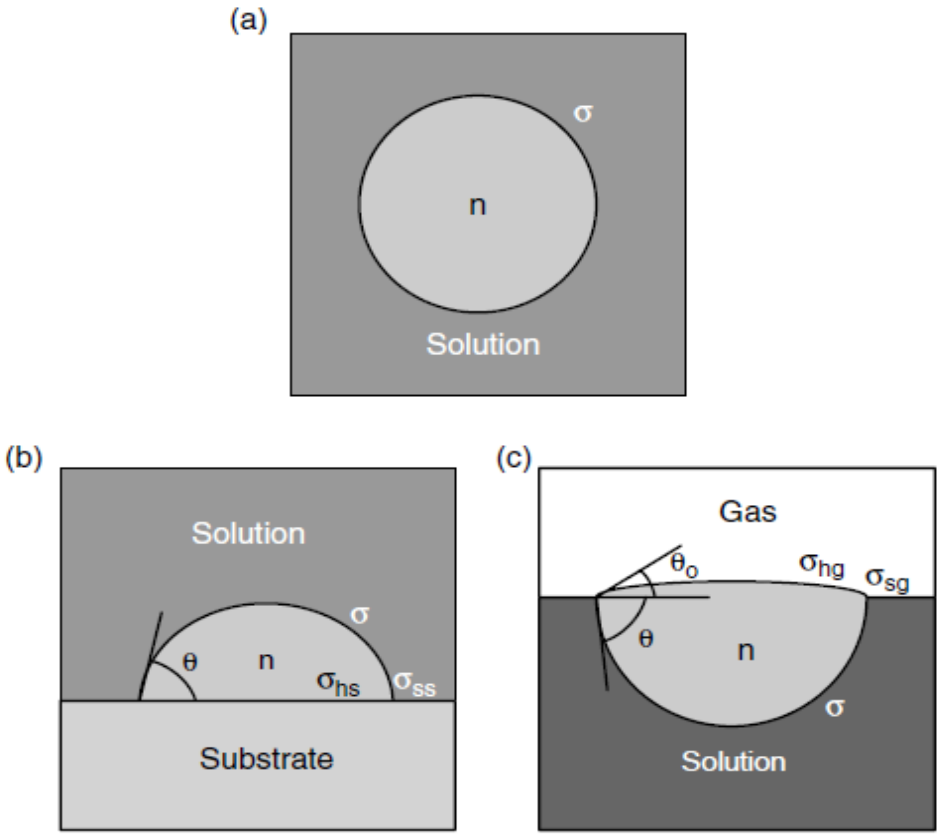

- **Figure 2.6.3: Conceptual picture showing the contact angle (Θ) between the surface and hydrate crystal for a) a spherical cluster in HON, b) a cap-shaped cluster in HEN on a substrate, c) a lens-shaped cluster in HEN at the solution-gas interface [23]**

The lower activation energy in heterogeneous nucleation results from not requiring energy to construct a surface for the clusters to grow on, as a surface already exists (cell wall etc.). Then logically HON requires higher activation energy because of the extra energy needed to create a surface. A comparison of HON and HEN made by Hanna Vehkamäki states that while the activation energy is different in both fore mentioned cases, the critical radius of the clusters are the same [29]. The number of molecules that participate in the critical size cluster for HEN however is smaller. This is shown in the figure on next page.

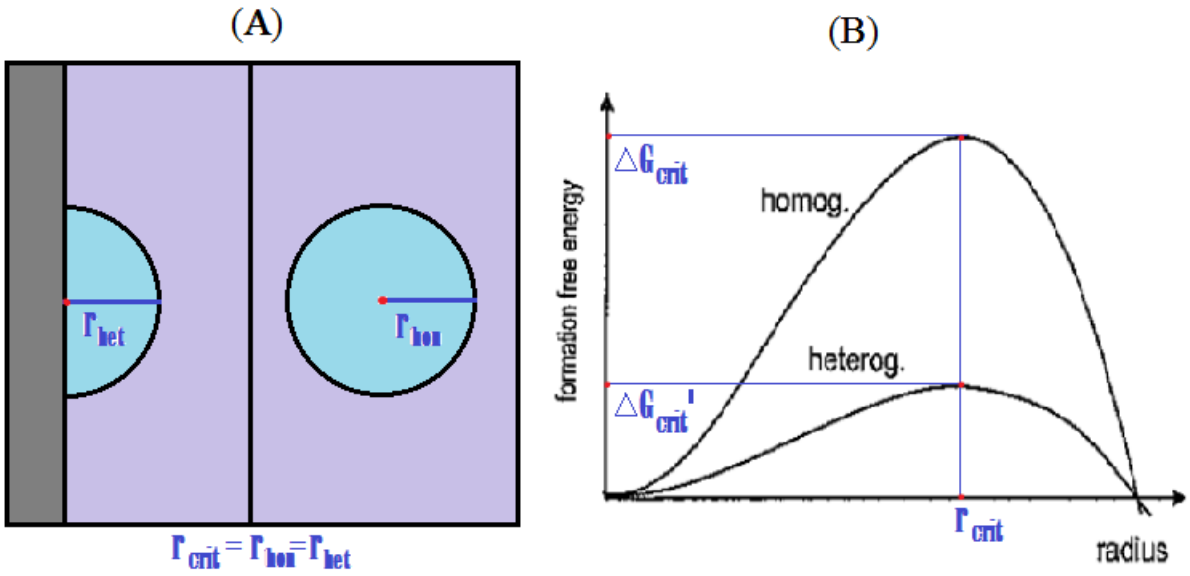

- **Figure 2.6.4: A) Illustration of radius for a critical sized cluster in heterogeneous nucleation, and radius for a critical sized cluster in homogenous nucleation. It is shown that these radiuses are equal. B) Activation energy as a function of radius for a cluster in homogenous- and heterogeneous nucleation. It is shown that the radiuses are equal, while the activation energies are different. (Modified graph) [29]**

The elapsed time from the start of experiments to the onset of hydrate formation is defined as the induction time. [30] Clusters having obtained a critical radius may be too small to observe at first experimentally until they have grown for some time. The nucleation may therefore occur before the first visible sign of hydrate in the system. The induction time is hard to derive explanations from, as it is a stochastic phenomenon. It can vary from just a few seconds or up to several hours for the same hydrate. It is therefore not an easy task to find a connection between physical measurable properties and the induction time.

2.7: Hydrate nucleation at the molecular level.

Molecular models of hydrate nucleation mainly focus on initiation of hydrate formation at the vapor-liquid interface, as this is most common. Below, three conceptual pictures of hydrate nucleation at the molecular level will be thoroughly explained. They are:

- The labile cluster nucleation hypothesis
- Nucleation at the interface hypothesis
- Local structuring nucleation hypothesis

The labile cluster hypothesis: The definition of a labile cluster is an unstable being that easily undergoes change. They are composed of a guest molecule that is surrounded by 20 and 24 (for cavities in sI) or 20 and 28 (for cavities in sII) water molecules in the first solvation shell. Nucleation is considered in this model to occur by the agglomeration of labile clusters either on the liquid or the vapor side of the interface.

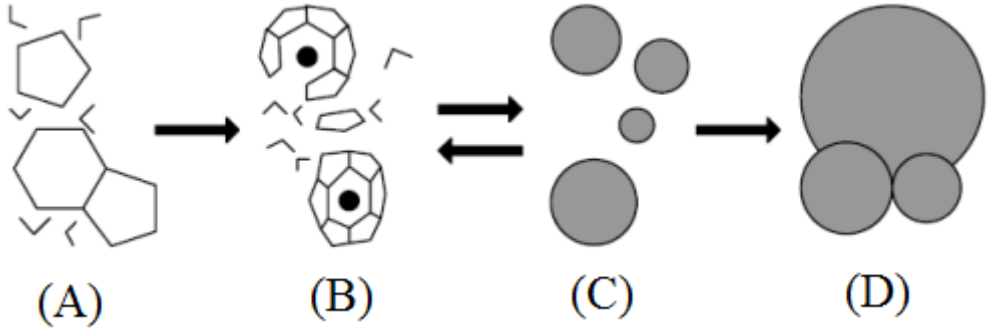

- **Figure 2.7.1: Agglomeration of labile clusters. A) Initial condition: Pressure and temperature in hydrate forming region, but no gas molecules dissolved in water, B) Labile clusters: Upon dissolution of gas in water, labile clusters form immediately, C) Agglomeration: Labile clusters agglomerate by sharing faces, thus increasing disorder, and D) Primary nucleation and growth: When the size of cluster agglomerate reaches a critical value, growth begins [23]**

Nucleation at the interface hypothesis: This is a modification of the hypothesis above, and is based on adsorption and clustering on the vapor side of the interface. In this model, gas molecules are transported to the interface where gas adsorbs to the aqueous surface. In the next step, gas molecules migrate to a fitting location for adsorption through surface diffusion. Partial cavities are formed first by water molecules at this location, before they evolve into complete cavities that trap the adsorbed species. Labile clusters take part and grow on the

vapor side of the interface until a critical size is obtained. There are two ways this can happen. The first is by addition of water and gas molecules to the already formed cavities. The second is via the joining of cavities along the interface. It is also possible that this happens as a combination of both ways.

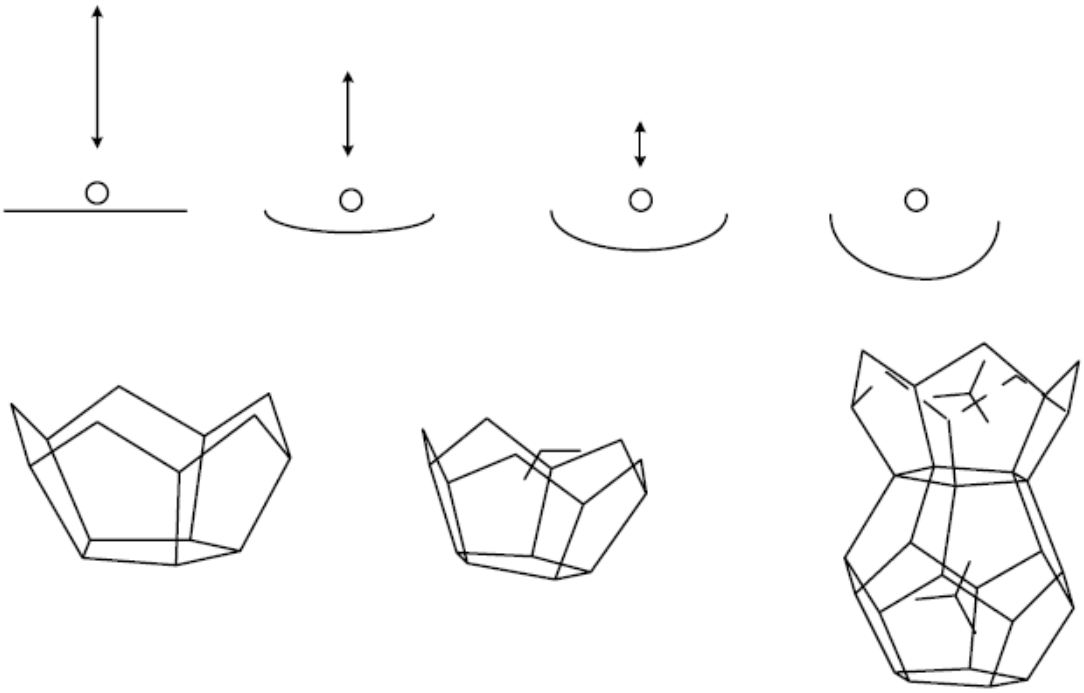

- **Figure 2.7.2: Gas molecules are adsorbed onto labile hydrate cavities at the interface between gas and water [23]**

Local structuring nucleation hypothesis: This model was developed more recently compared to the other two hypotheses. It focuses on the development of guest molecules being ordered in configurations that bear resemblance to that in the hydrate and a hydrogen-bonded water network. [23] Radhakrishnan and Trout performed free energy calculations to study the homogenous nucleation mechanism of carbon dioxide (CO_2) hydrate at the interface between liquid water and liquid gas. These calculations showed that it was more favorable (thermodynamically) for labile clusters to disintegrate than to agglomerate. Because of this, Radhakrishnan and Trout suggested that the possibility of carbon dioxide hydrate nucleation to occur via the labile cluster hypothesis was virtually zero and proposed the local structuring hypothesis. In this hypothesis, a group of guest molecules (CO_2) are arranged in a configuration similar to that in the clathrate hydrate phase caused by thermal fluctuations. The

structure of water molecules surrounding the locally ordered guest molecules is perturbed compared to the bulk. The finite temperature of the system causes the thermodynamic perturbation of the liquid phase, which is a stochastic process. The number of molecules in the critical cluster is exceeded by the amount found in a locally ordered arrangement. The cluster order parameters for guest-guest and host-host take on values that are very similar to the clathrate hydrate phase, which leads to forming a critical size cluster. [31] Other models similar to this hypothesis also exist.

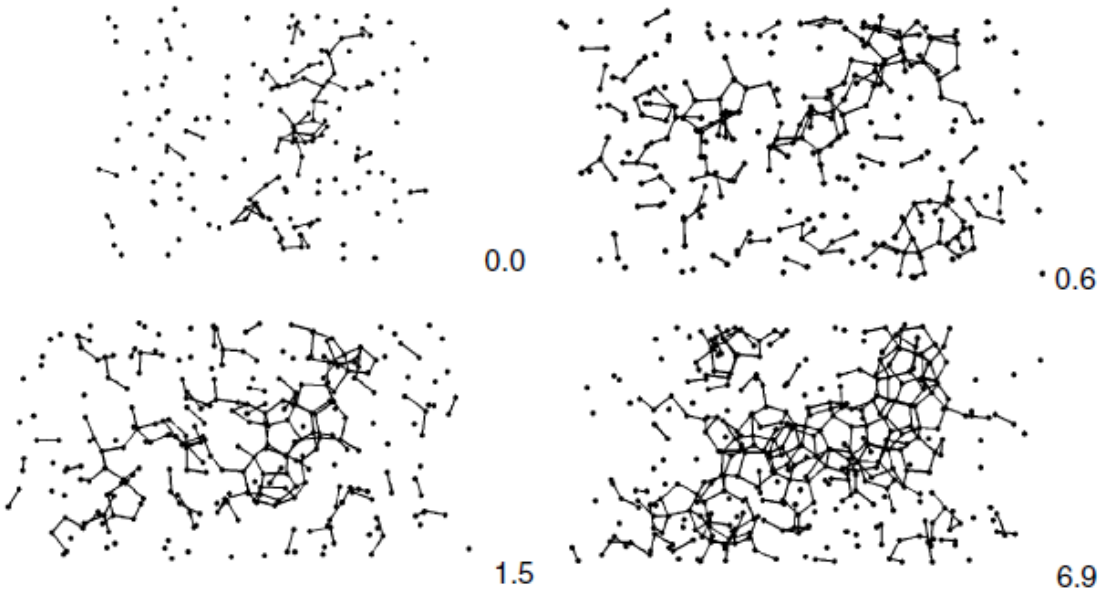

- **Figure 2.7.3: Clathrate hydrates shown at different times (ns). The lines represent the hydrogen-bond network. Hydrate-like waters are shown only. One can clearly see that a complete cavity have been formed after 1.5 ns, and that many more complete cavities also have been formed after 6.9 ns [23]**

The different hypotheses each explain nucleation at the molecular level in different ways. There is however a possibility that the nucleation process occurs via some kind of combination of these hypotheses. [23]

2.8: Subcooling as the driving force of nucleation.

Several driving forces exist for hydrate nucleation. Limited proof associating the driving forces with equilibrium/nonequilibrium thermodynamics exist, with the exception of a few works. A list of the driving forces for the nucleation process is given below.

- **Table 2.8.1: The driving forces of nucleation (reproduced table) [23]**

Researchers	Year	Driving force
Vysniauskas and Bishnoi	1983	$T^{eq} - T^{exp}$
Skovborg and Rasmussen	1992	$\mu^{exp}_{WH} - \mu^{exp}_{WL}$
Natarjan et al.	1994	$f_i^{exp}/f_i^{eq} - 1$
Christiansen and Sloan	1995	Δg^{exp}
Kashchiev and Firoozabadi	2002	$\Delta \mu$
Anklam and Firozabadi	2004	Δg
Arjmandi et al.	2005	$T^{eq} - T^{exp}$

The most important part of the correlation for hydrate nucleation is the driving force. [23] The driving force is necessary to overcome the nucleation barrier (reach the activation energy). [32]

Christiansen and Sloan proposed the change in total molar Gibbs free energy (Δg^{exp}) to be the real driving force, and it has been shown that this is the general case for all other driving forces of nucleation proposed by previous researchers. [23]

A driving force that is comprehensive for the formation of hydrate is a function of pressure, temperature and composition of gas and is of great importance when it comes to the description of the appearance and growth of gas hydrates. As the calculations for such a driving force is complicated, the degree of subcooling is mostly used as the driving force of formation of hydrate because of its much simpler calculation.

Subcooling is given as:

$$\Delta T = T^{eq} - T^{exp} \qquad (2.8.1)$$

That is, equilibrium temperature (T^{eq}) minus the experimental temperature (T^{exp}) at the experimental pressure (P^{exp}). ΔT is the subcooling (illustrated in figure 2.8.1).

A drawback with subcooling is that it does not take into account the effect of pressure. Arjmandi et al. showed that subcooling is proportional to the driving force for pure gas-water systems (methane as single hydrate former in their case) at a wide pressure range. For multicomponent systems (natural gases) however, the real driving force is somewhat underestimated by subcooling. In these systems, subcooling could be a good measure of the driving force at some pressure ranges but underestimated at others. [30]

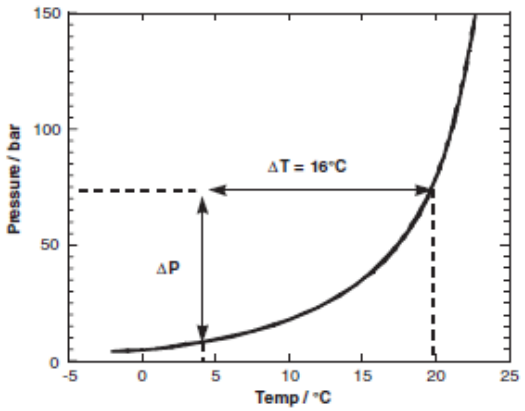

- **Figure 2.8.1: PT diagram illustrating the subcooling, ΔT, for a gas hydrate at 4°C and 75 bar. The left side of this curve represents the hydrate formation region, where the temperatures and pressures are in favor of hydrate formation. Hydrate formation is not possible on the right side of this curve, whereas the curve itself represents the equilibrium temperatures and pressures for hydrate formation [33]**

In this thesis, subcooling is taken as the driving force of hydrate formation. It may however be incorrect to assume such a driving force for the experiments done with the synthetic natural gas if we consider the facts above. On the other hand, subcooling seems to be a good representative of the driving force for the experiments done with the pure methane gas.

It was observed from the experiments with both pure methane and SNG-7 that an increasing ΔT resulted in shorter induction times. This is logical, since we are further inside the hydrate formation region where nucleation will occur faster.

The cooling rate has also an effect on the nucleation rate (number of stable clusters formed per unit volume and per unit time) for systems with SNG-7, as it was observed that a reduced cooling rate resulted in an increased nucleation rate. The reason for this being that the clusters will have more time to form and dissolve, as the system stays longer in the hydrate forming region than at a higher cooling rate. [34]

2.9: Kinetic hydrate inhibitors.

Kinetic hydrate inhibitors (KHI`s) are low molecular weight polymers dissolved in a carrier solvent which are injected into the water phase in the pipeline. This type of inhibitor prevents plug formation for a while longer than the free water residence time in a pipeline by bonding to the hydrate surface. The presence of hydrocarbons (liquid phase) is not necessary for this method of hydrate prevention to be effective.

KHI slow down the hydrate formation rather than make it thermodynamically impossible, which is the case with thermodynamic hydrate inhibitors [35].

KHI`s are limited at long times, high pressures and low temperatures. Given enough time, as the concentration of KHI decreases, the crystal growth will become sufficient to create plugs in pipelines.

They are, as explained in the introduction of this thesis, low dosage inhibitors (LDHI`s), meaning that they are effective at much lower concentrations than thermodynamic inhibitors (MEG, MeOH).

Some of the kinetic hydrate inhibitors are shown in the figure below.

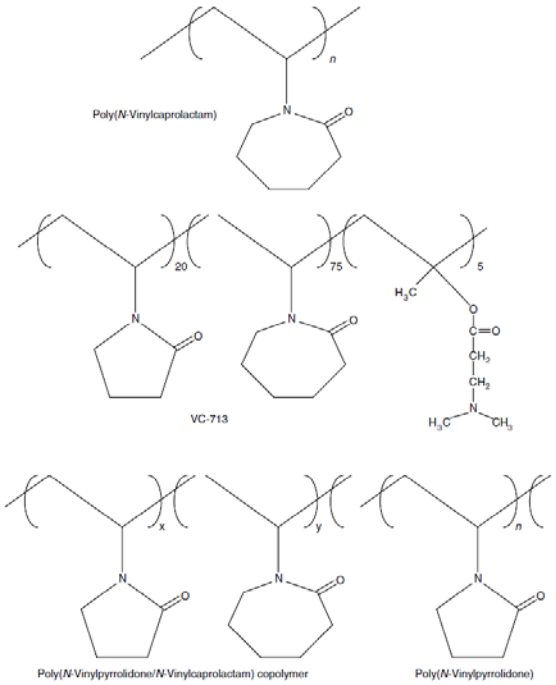

- **Figure 2.9.1: Kinetic hydrate inhibitors. Angles are locations of a carbon atom (if nothing else indicated) [3]**

From figure 2.9.1 on the previous page, the inhibitors are shown to have a polyethylene backbone, from which a pendant group (typically a ring compound with an amide [-N-C=O] linkage) is supended.

The effectiveness of KHI`s are limited to a subcooling, ΔT, of approximately 20 ^{o}C. Subcooling is directly proportional to the surface tension σ between liquid and hydrate crystal, but inversely proportional to the length L between polymer strands.

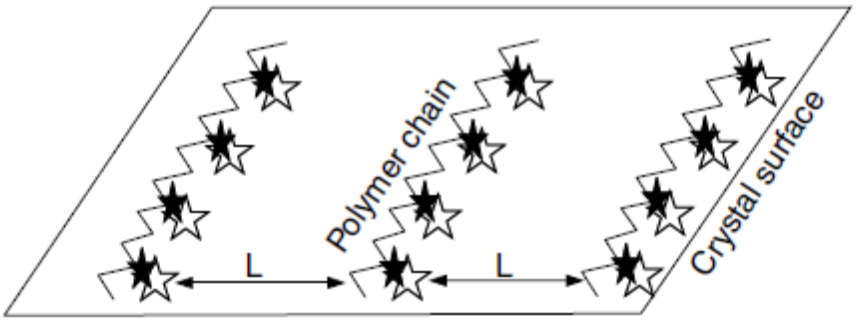

- **Figure 2.9.2: A KHI mechanism [3]**

The KHI mechanism shown in the figure above is explained by:

$$\Delta T \leq \frac{4\sigma}{CL} \qquad (2.9.1)$$

The C in the equation is a constant.
Using equation (2.9.1) we can see that:

- The subcooling performance increases if the amount of polymer adsorption increases and the length between the polymer strands decreases
- On the other hand, a reduction of subcooling performance will be the result if the amount of polymer adsorption decreases and the length between polymer strands increases

One of the best KHI`s was developed by ExxonMobil, the N-methyl-N-vinylacetamide:polyisopropyl-methacryalamide 1:1 low molecular weight copolymer (VIMA:IPMA 1:1). This KHI is effective up to a subcooling, ΔT, of 23^{o}C. A drawback with

this inhibitor is its high cost and low availability. As many other KHI`s exist, only the two kinetic inhibitors that have been used in this thesis will be explained in details:

- PVP (Poly-N-vinylpyrrolidione)
- PVCap (Poly-N-vinylcaprolactam)

One of the first KHI developed was PVP. It is only effective at subcoolings up to 5^{o}C, making it the weakest of the KHI`s. [3] Molecular dynamic simulations suggest that PVP disturbs the water structure and slows down/reduces nucleation. As the hydrate is formed, PVP removes itself from the hydrate surface without creating any bonds between the hydrate and PVP. According to this, PVP only works on the nucleation phase and not on the growth phase. [36]

PVCap on the other hand, is a more effective KHI that works at subcoolings up to 8-9 ^{o}C. [3] From molecular dynamic simulations it seems that PVCap structure the water in a hydrate like pattern around the lactam-ring. Molecular dynamic simulations also show that PVCap is attracted to the hydrate surface, and creates bonds there. According to this, PVCap seems to work as a promoter on the nucleation phase and as an inhibitor on the growth phase of the hydrates. [36]

PVP with molecular weight, M_w = 15000 Daltons, and PVCap with molecular weight, M_w = 6000 Daltons, was used in the present study. Both were used in concentrations of 50 ppm based on the water phase.

2.10: Growth phase of hydrates.

When the nucleation phase of hydrates is finished, the growth phase begins. Unlike the stochastic nature of the nucleation from which deriving anything from is hard, the growth phase is more easily understood and modeled.

The parameters which are important for the nucleation phase are also important for the growth phase. These parameters include the displacement from equilibrium conditions, water history, surface area, agitation and gas composition.

Two processes become very essential during the growth:

- The mass transfer: Transport of components to the growing crystal surface
- The heat transfer: Transport of the exothermic heat of hydrate formation away from the growing crystal surface

From the molecular level of perspective, the growth of hydrates can be thought of as a combination of three factors (1.heat- and 2.mass transfer). The third factor is the kinetics of crystal growth at the hydrate surface.

A hypothetical picture of a hydrate growing at a crystal is shown below:

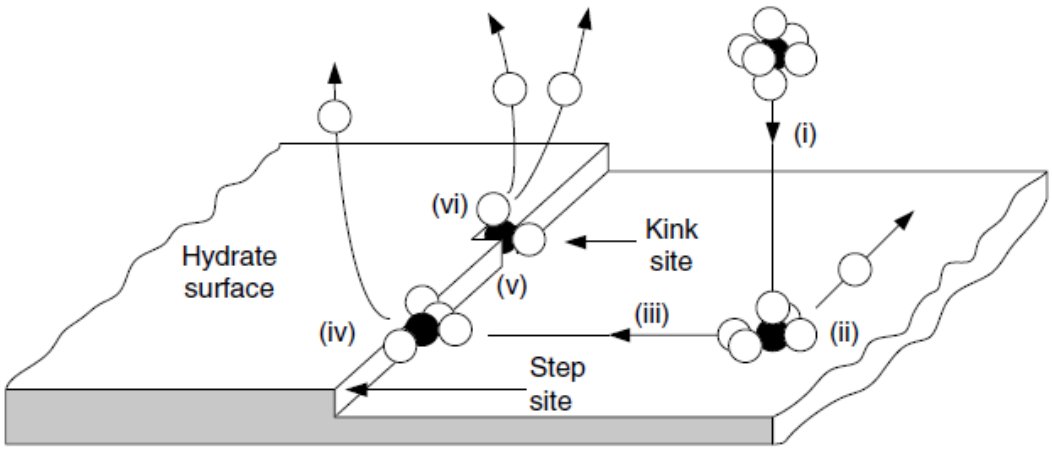

- **Figure 2.10.1: Growth of hydrate at a crystal (hypothetical picture) [23]**

The steps in figure 2.10.1 are described below:

- Step i: A guest in a temporal water cluster is transported to the growing crystal surface. The lower Gibbs free energy provided at the crystal surface drives the cluster to the surface
- Step ii: The cluster adsorbs onto the crystal surface. The cluster adheres to the surface due to a force field exerted by the solid crystal. Some of the water molecules detach from the crystal and diffuse away upon adsorption
- Step iii: The cluster diffuses over the surface to a step in the crystal. Because the solid force field is perpendicular to the crystal face, the adsorbed species can diffuse only in two dimensions along the surface
- Step iv: The cluster attaches to a crystal step, resulting in further release of solvent molecules. The step is an attractive site because two solid faces on the step exert a force (with two surface-reactant interactions) on the mobile species, in contrast to a single force field (with one surface-reactant interaction) on the flat surface
- Step v: Movement of the cluster is restricted to a single dimension along the step. It diffuses along the step to a kink or defect point in the step
- Step vi: The cluster adsorbs at the kink. The kink is an attractive site because three or more solid faces of the kink exert a larger force on the species than the two forces exerted by the step alone
- Step vii (not shown in the figure): The cluster is now immobilized in three dimensions

Integration of the cluster into the crystal surface takes place in the first 3 steps. The cluster rearranges itself into the proper cavity and excess solvent molecules are released. If the guest molecule is too large for a cavity, it may take some time for the cavity to rearrange itself (C_3H_6 is for example too large to fit into a 5^{12}-cavity). A rate-limiting step can be the water rearrangement into the proper cavity.

Using Avogadro`s number of molecules participating in the process described in figure 2.10.1, it would not be right to make the assumption that all molecules progress through the above steps in a deterministic way. Every possible combination of attachment is tried due to the high number of molecules in motion. An example of this could be a cluster attaching itself directly to the kink without any significant diffusion.

Experiments conducted on hydrate growth have given little verification of the hypothetical model presented in figure 2.10.1. Still it serves as a good idea on how the process of hydrate growth takes place, and can be a basis for further improvement to create an even better growth model. [23]

3. **Experimental setup and method.**

The experiments were performed in 3 closed cells (Cell #1, Cell #2, Cell #3), in which gas hydrates were formed.

Three other students conducted their MSc and BSc experimental work in the hydrate lab during the spring semester. Results from their work have been applied for analysis in the present MSc thesis. These are: Magnus Palm (MSc), Silje Bru (BSc) and Leif Inge Kjærvoll Sørskår (BSc). A minimum number of 6 parallel experiments are required to obtain sufficient statistical accuracy of analysis. Thus the possibility to utilize data produced from others has been for the evaluation of the applicability and accuracy of the experimental method used.

Since the experimental pressure was kept constant the driving force of the system was assumed to be represented by subcooling, ΔT, during each experimental series at given pressure.

Hydrate nucleation experiments were conducted using distilled water with and without KHI and synthetic natural gas (SNG-7) only in two of the cells (#1 and #3), and pure methane gas and distilled water without KHI only in Cell #2. The SNG-7 contains components that form hydrate structure II (sII), while pure methane form hydrate structure I (sI).

Experiments on pure distilled water without any additives were used for baseline measurements. Each experimental set conducted at given pressure consisted of totally 18 experiments as minimum at a minimum of three different temperatures. A minimum of six experiments were conducted at each experimental temperature. Additional experiments were carried out if the 6 experiments done for a temperature seemed insufficient for reliable statistical analysis. The hydrate nucleation process is stochastic and in some cases six experiments are too few to cover the time window where nuclei formation would occur most frequently at given experimental conditions. Ideally the number of experiments within a set of parallel experiments should probably be around 15 to 20 or even greater. Such amount of experiments was beyond the time frame of this MSc thesis and we have tried to keep the number of experiments at a minimum without coming in conflict with the accuracy and reliability of the method used.

Experiments on pure methane in Cell #2 were done on pure distilled water without KHI only, because the MSc topic of the executing candidate, Magnus Palm, did not involve effects of KHI. This series was conducted at a fixed experimental pressure of 90 bar, and experimental temperatures of 6, 7 and 8 ^{o}C.

Five series of experiments were conducted in Cell #3, of which two were done by Silje Bru as part of her BSc thesis work. These two series were conducted at a constant experimental pressure of 61 bar, and at experimental temperatures of 11, 12 and 13 ^{o}C using distilled water during the first series, and distilled water added the kinetic inhibitor PVP-K15 in the second series. PVP-K15 means a PVP polymer having a molecular weight, M_w, of 15000 Daltons (M_w = weight average molecular weight). The concentration of PVP was 50 ppm in the aqueous phase. The remaining 3 series performed in Cell #3 was made by me. These series were performed at a constant experimental pressure of 90 bar, and experimental temperatures of 13, 14.25 and 15.5 ^{o}C. Distilled water was used in two of the series, while the kinetic inhibitor PVCap-6k was used in the third series. PVCap-6k means a PVCap polymer having a molecular weight, M_w, of 6000 Daltons. The concentration of PVCap was 50 ppm in distilled water in all PVCap experiments.

Three experimental series were conducted in Cell #1, two of them done by Leif Inge Kjærvoll Sørskår as part of his BSc thesis. These series were conducted at a constant experimental pressure of 61 bar, and experimental temperatures of 10, 10.5 and 11 ^{o}C. Distilled water was used in the first series, and the kinetic inhibitor PVCap-6k (50 ppm) in the other. The third series was made by me, and was a reproduction of the baseline series as conducted in Cell #3 at an experimental pressure of 90 bar.

An overview of the responsible candidate for the performance of the various experiments included in the present data analysis is shown in table 7.1 in the appendix.

An outline of the experimental setup used in this thesis is shown in figure 3.1. The main constituents of the experimental system are:

- Temp Control unit: (Cooling/-heating bath): Julabo F34 and F33, with temperature stability of ±0.01^{o}C

- Pressure sensor: Rousemount TA3051TA absolute pressure transducer, 0-276 bar absolute, accuracy: ±0.025 bar up to 100 bar, thereafter 0.025% of the full scale
- Temperature probes: Pt-100 with an accuracy of 1/10 DIN (±0.03 ^{o}C at the freezing point of water)

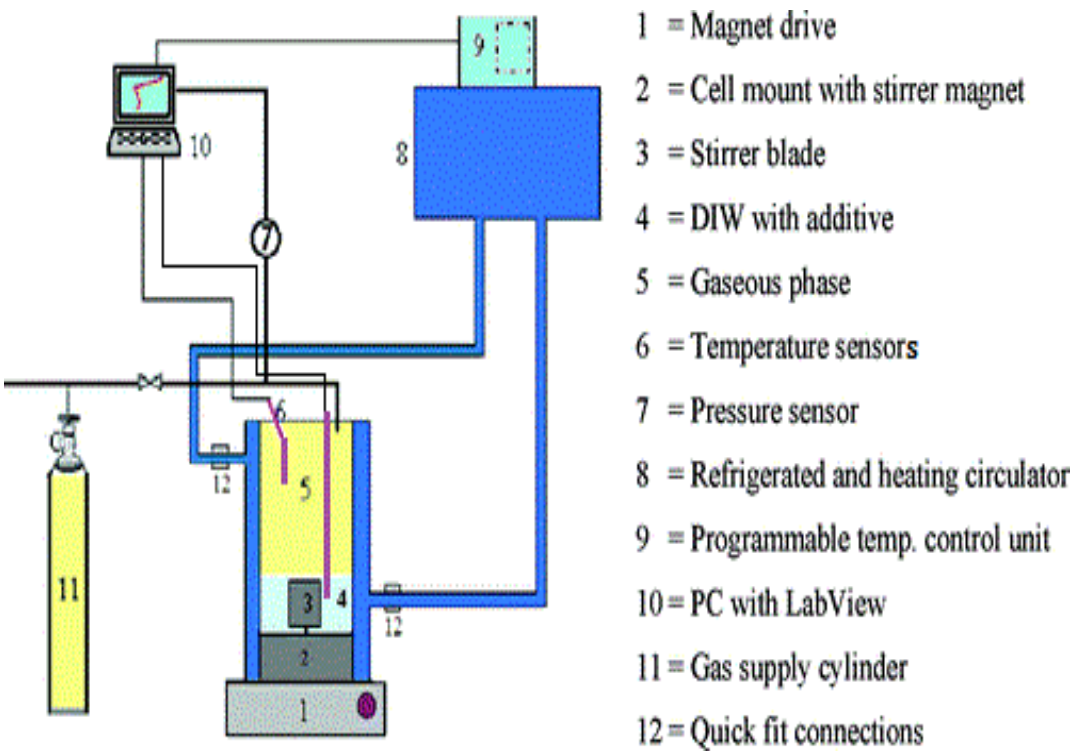

- **Figure 3.1: Schematic showing the experimental cell and equipment (modified to include 2 temperature sensors) [37]**

3.1: The experimental cells.

The cells used in the experiments are made of titanium with inner volume of 141,4 ml. The cells consist of a cooling cap, cell wall, stirrer blade, top lid, temperature sensors, gas supply tubing, bottom lid, stirrer magnet, o-rings, and a nylon bit (nylon was only used in Cell #1 and #2 in order to raise the stirrer blade high enough to prevent it from scratching the bottom of the cells). The cell walls had a smooth surface while the stirrer blade surface was plain, but not smooth. The temperature sensors were encapsulated in 316 stainless steel tubing with smooth surface. The top lid had a smooth inner surface while the cell bottom had fine, circular scratches produced by stirrer blade at too low position in previous experimental work by other

candidates. The smoothness and quality of surfaces in contact with the hydrate forming phases could affect the nucleation process through various and unknown/undetermined processes.

The cells also have the possibility to be connected to a cooling bath, in order to cool down or heat up the cells. The figure below shows the different parts the cells are made up of.

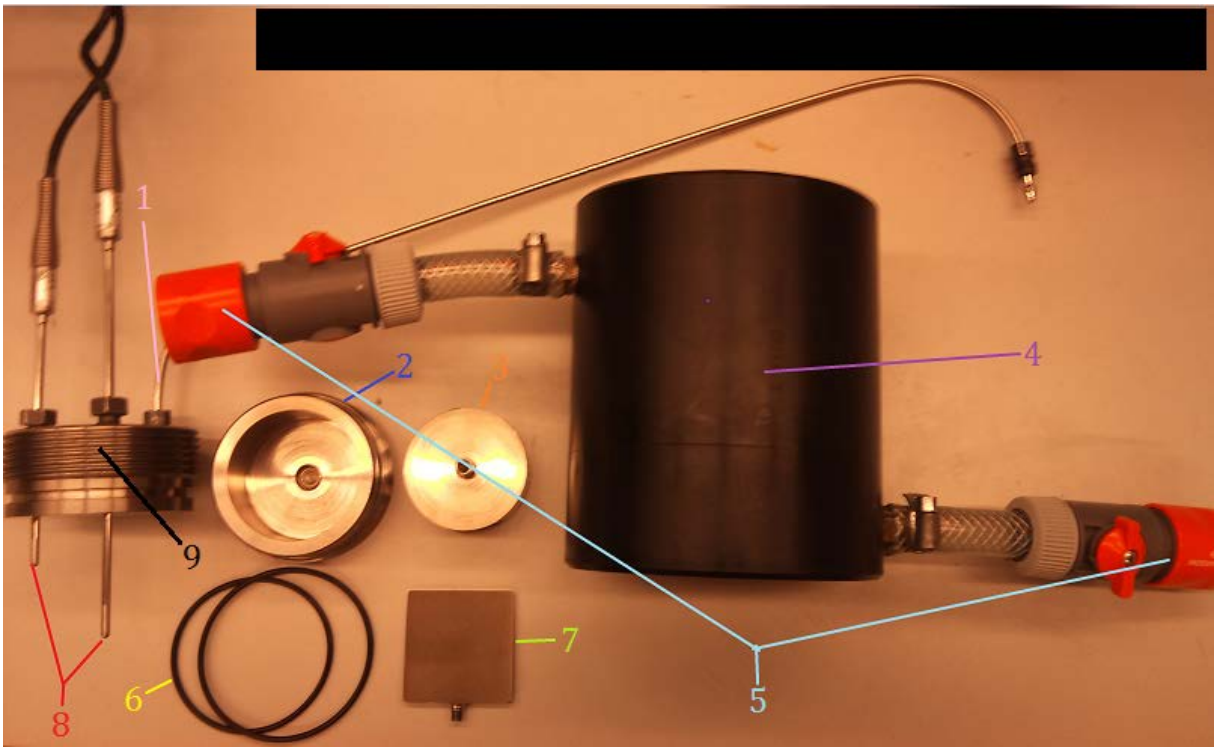

- **Figure 3.1.1: Dismantled experimental cell**

1. Gas supply tubing
2. Bottom lid
3. Stirrer magnet
4. Cooling cap
5. Connections to cooling bath
6. O-rings
7. Stirrer blade
8. Temperature sensors
9. Top lid

3.2: The cooling baths.

The function of the cooling baths is to cool down or heat up the experimental cells. It is connected to the cells through the circulatory system shown in figure 3.1.1. The cooling baths can be programmed to follow any necessary temperature profiles. The program can contain up to 60 regulation steps per regulation loop, and every loop can be repeated up to 6 times before the program ends. The cooling baths are shown in the figure below. Initially the system was connected to the Julabo F34 HL bath. This was replaced by Julabo F33 HL bath approx. midways during the experimental series due to cooling fan failure in the F34 baths. The baths have identical cooling capacity and temperature stability. The main difference is a cooling liquid volume of 20 liters for F34 and 16 liters for F33.

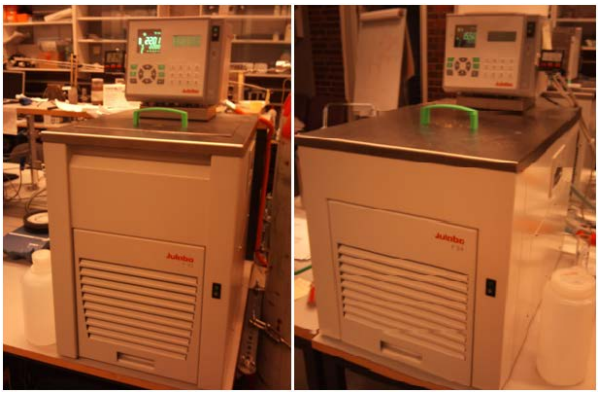

- **Figure 3.2.1: The cooling baths. Model: Julabo F33 (Left) and Julabo F34 (right)**

3.3: SNG-7 and pure methane.

Two gases were used in the experiments:

- SNG-7 (Synthetic Natural Gas 7 components), composition is showed in table 3.3.1
- Methane, scientific purity grade of 5,5 which corresponds to a purity of 99,9995%

- **Table 3.3.1: Composition of the SNG-7 used in most of the experiments conducted in the present study**

Component	Spesific composition [mol%]
Methane	80,4
Ethane	10,3
Propane	5
i-butane	1,65
n-butane	0,72
CO_2	1,82
Nitrogen	0,11
Sum	100

3.4: Cell assembly.

The following procedure was followed when assembling the cells before the start of experiments:

1. The stirrer blade- and magnet was screwed together through a hole that connects the inside of the upper part of the cell with the inside of the bottom part of the cell
2. O-rings were attached to the top- and bottom lids
3. The bottom lid of the cell was then filled up with distilled water or KHI (approx. 1/5 of the bottom lid volume). The bottom lid was screwed into the bottom part of the cell. The distilled water/KHI would then squeeze out unwanted air, leaving a fluid at the inside of the upper part of the cell. The remaining fluid was removed
4. The cell was placed on a magnet drive
5. The inside of the cell was then filled up with 50 ml of distilled water/KHI
6. The top lid was screwed into the cell
7. The cell was connected to the cooling bath
8. The gas supply tubing was connected to the gas supply cylinder

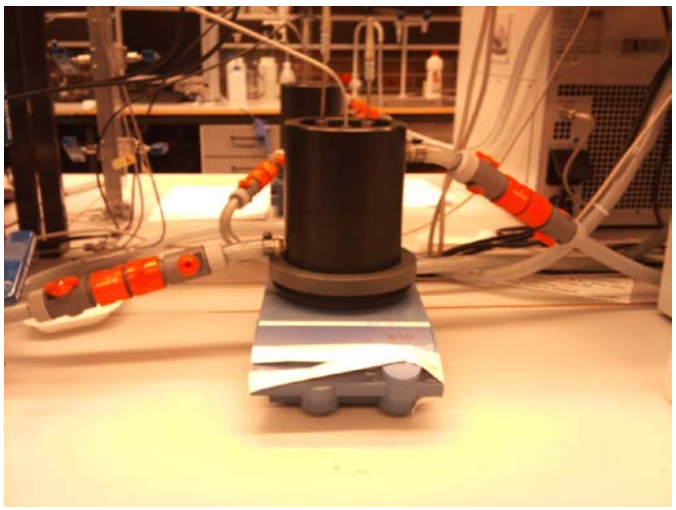

- **Figure 3.4.1: Assembled experimental cell placed on a magnet drive**

3.5: Gas filling procedure.

The experimental cells were filled up with gas after being assembled. As mentioned earlier in this thesis, both a synthetic natural gas and pure methane was used for the experiments. Both the gas supply cylinder containing SNG-7 and the gas supply cylinder containing pure methane were connected to a system which again was connected to the cells. The following procedure for gas filling was used in the experiments:

1. The remains of air had to be driven out of the cells. This was done by purging the cells with 40 bar SNG-7/methane. The process of purging was carried out twice per experiment, diluting the remaining air in the cells by a total of 1600 times (40*40)
2. The cells were filled up with SNG-7/methane to the desired starting pressure after the process of purging

It was checked for possible gas leakages from the cells before the start of the experiments.

3.6: Execution of experiments.

After assembling, purging and filling the cells with gas to the stable desired pressure at starting temperature the experiments could begin. Every experiment conducted in this thesis followed the same procedure. They started with keeping the temperature constant at the desired starting pressure for 10 minutes. After this, the system was cooled down with a constant cooling rate until the desired experimental temperature was reached. The starting pressure in the cell was calculated through regression analysis, so that when the cooling was finished the experimental pressure would be reached. The temperature in the gas and water phase was a little behind the temperature in the cooling bath when it came to reaching the experimental temperature, so the system was left alone for 5 minutes to adjust itself after the end of cooling. The stirring mechanism began when those 5 minutes were over, marking the starting point of the experiments.

The experiments ran until hydrate was formed in the cells. After this the experiments were ended and the cells warmed up to starting temperature.

The gas in the cells was released after the melting of hydrate and stop of stirring mechanism. After this the cells were dismantled, remains of distilled water/KHI removed, and the cells thoroughly washed.

Each person that conducted experiments in the present study kept the starting temperature, experimental pressure, cooling rate, and stirring rate constant for their own experimental series, but used different values for these compared to the others. The starting temperature was a little higher than the equilibrium temperature of the system, so that no hydrate could be formed before the start of experiments.

A list of some other experimental differences in addition to the ones mentioned above is shown below:

- Stirring rate
- Cooling rate
- Starting temperatures and pressures
- Experimental temperatures and pressures
- Type of gas

3.7: The nucleation probability distribution function.

Using a deterministic approach to explain the nucleation process of hydrates is inappropriate due to the random nature of nucleation. Instead, it is more accurate to use a probabilistic approach.

The Poisson distribution law gives the probability, P_m, of forming m clusters during a time interval, ΔT. The Poisson distribution law is as follows: [38, 39]

$$P_m = \frac{N^m e^{(-N)}}{m!} \qquad (3.7.1)$$

In this formula, N as a function of t is the average expected number of clusters formed during the time interval Δt. The probability of forming zero clusters (P_0(m=0)) is:

$$P_0 = e^{(-N)} \qquad (3.7.2)$$

Whereas the probability of forming one cluster (P_1(m=1))is:

$$P_1 = Ne^{(-N)} \qquad (3.7.3)$$

The probability to form m or more clusters during the time interval Δt is represented as:

$$P_{\geq m} = 1 - P_0 - P_1 - P_2 - \cdots - P_{m-1} = 1 - \sum_{i=0}^{m-1} P_i \qquad (3.7.4)$$

From equation (3.7.1) and (3.7.4) we get:

$$P_{\geq m} = 1 - e^{(-N)} \sum_{i=0}^{m-1} \frac{N^i}{i!} \qquad (3.7.5)$$

Using the equation above, setting $P_{\geq 1}$ as the probability we get:

$$P_{\geq 1} = 1 - P_0 = 1 - e^{-N} \qquad (3.7.6)$$

The stationary nucleation rate J is related to the average number of clusters N that have been formed during the time interval Δt in the following way:

$$N = JV\Delta t \qquad (3.7.7)$$

By implementing the right hand side of equation (3.7.7) into equation (3.7.6), we get the probability of forming at least one cluster during the time interval Δt, P'(Δt):

$$P'(\Delta t) = 1 - e^{-JV\Delta t} \qquad (3.7.8)$$

Because detecting a cluster demands that the cluster formed in a solution have to grow to a detectable size, a time delay called the lag time τ_0 occurs between the time Δt of appearance of a cluster and the time t of detection called the induction time. The lag time τ_0 is the measure of the time necessary for the nucleation rate to attain a steady state value. It is represented as:

$$\Delta t = t - \tau_0 \qquad (3.7.9)$$

Implementing equation (3.7.9) into equation (3.7.8) we get the probability of detecting hydrate crystals at time t which were nucleated at an earlier time, P(t):

$$P(t) = 1 - e^{-JV(t-\tau_0)} \qquad (3.7.10)$$

The above cumulative distribution function is valid for times $t \geq \tau_0$. [40] The probability of detecting hydrate crystals per unit volume at time t which were nucleated at an earlier time, P(t):

$$P(t) = 1 - e^{-J(t-\tau_0)} \qquad (3.7.11)$$

The above equation is called the nucleation probability distribution function. [41] The probability distribution function can be applied to analyze nucleation experiments in general and for gas hydrates especially. [37] This function was applied to analyze the experiments carried out in this thesis, in order to determine the nucleation rates and lag times.

3.8: The Arrhenius equation.

Many equations developed experimentally relating the rate constant k of a chemical reaction to the temperature T appeared during the middle of the 19th century and outwards. These equations gave approximately linear fits of the data, but this was due to the narrow temperature range employed in the kinetic studies. If a wider temperature range was used for these equations, the linearity of the fit with the data decreased. This resulted in all of those equations being dropped, except for two of them: [42]

- The Arrhenius equation
- The modified Arrhenius equations

Svante Arrhenius was the first to use the Arrhenius equation. He used it in his studies of the dissociation of electrolytes [43]. It is today a widely accepted tool in describing the influence of temperature on the rates of chemical processes and also for many other physical processes, such as thermal and electrical conductivity, viscosity and diffusion.
The Arrhenius equation is represented as:

$$K = Ae^{\left(-\frac{E_a}{kT}\right)} \qquad (3.8.1)$$

Where K is the rate of reaction (s^{-1}), A is the pre-exponential factor, E_a is the activation energy (J), k is the Boltzmann constant ($1.3806505*10^{-23}$ J/K), and T is the experimental temperature (K). [42]
If k is replaced with R (the gas constant, 8.3145 J/K mol) in the Arrhenius equation, the activation energy E_a will come out with the units of J/mol.
By taking the natural logarithm (ln) of the Arrhenius equation, the Arrhenius becomes:

$$\ln(K) = \ln(A) - \frac{E_a}{kT} \qquad (3.8.2)$$

If we rewrite eq. (3.8.2) into:

$$\ln(K) = \ln(A) - \frac{1}{T}\left(\frac{E_a}{k}\right) \qquad (3.8.3)$$

The Arrhenius equation becomes an equation for a straight line:

$$y = b - ax \qquad (3.8.4)$$

Where y is ln(K), b is ln(A), a is E_a/k and x represents 1/T.

The Arrhenius equation is also valid for describing the relationship between the temperature and rate of nucleation for gas hydrates. However, no studies have been conducted in finding the activation energy related to the formation of a critical size water cluster using this method. Researchers have instead focused on determining the activation energy at the point where hydrates start to grow self-sustainingly (as in [12] where Bergeron et al. calculated this type of activation energy to be -323 kJ/mol for methane). In the beginning of the growth phase, the system needs extra energy input in order for the growth to continue as the energy in the system alone is too small to sustain a growth. When a certain energy level is attained in the system, the growth of hydrate becomes self-sustaining, meaning no extra energy input to the system is needed for the growth to proceed.

The Arrhenius equation for describing the temperature dependence on the rate of nucleation for the hydrate formation process can be written as:

$$J = J_0 e^{\left(-\frac{E_{a1}}{kT}\right)} \qquad (3.8.5)$$

J is the rate of nucleation (s^{-1}), J_0 is the pre-exponential factor, E_{a1} is the Gibbs free energy barrier, ΔG, of the system, k is the Boltzmann constant, and T is the experimental system temperature. To form the critical size water cluster the system has to be lifted above the energy barrier, ΔG or ΔG_{crit} (often referred to as activation energy).
This can be written as eq. (3.8.3):

$$\ln(J) = \ln(J_0) - \frac{1}{T}\left(\frac{\Delta G_{crit}}{k}\right) \qquad (3.8.6)$$

Giving the final expression for finding the activation energy needed to form a critical size water cluster in the system before spontaneous growth of hydrate occurs. [32] One condition for using this equation is keeping the pressure constant and the temperature a variable.

Plotting ln(J) versus 1/T should ideally (according to Arrhenius theory) give a straight line. The slope of this line represents $\Delta G_{crit}/k$ and the energy barrier, $E_{a1} = \Delta G_{crit}$, can be determined by regression analysis provided measurements conducted at a minimum of three different temperatures. Achieving the value of the energy barrier is then done by simply multiplying the value of the slope with the Boltzmann constant k (ΔG_{crit} in J/unit cluster).

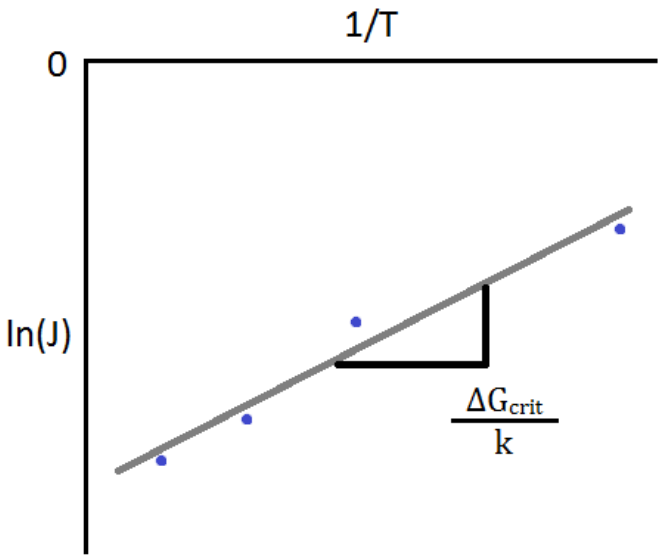

- **Figure 3.8.1: Schematic showing how ln(J) is plotted against experimental temperature using the Arrhenius equation**

One can then further use this energy barrier to calculate the radius of the critical size water cluster by using the general formula for classical nucleation theory.

$$\Delta G_{crit} = \frac{4\pi\sigma {r_{crit}}^2}{3} \qquad (3.8.7)$$

This equation is explained in section 2.6.

Rearranging eq. (3.8.7):

$$r_{crit} = \sqrt{\frac{3\Delta G_{crit}}{4\pi\sigma}} \qquad (3.8.8)$$

Using this equation, one can calculate the radius of the critical size water cluster. The surface tension is assumed to be 0.0276 J/m^2, which is the surface tension between ice and water.

This is often taken as a good approximation for the surface tension between hydrate and water.

It should be mentioned that the value of the assumed surface tension may deviate from reality. Zatsepina and Buffett used a lumped parameter model to determine the surface tension in their work on nucleation of CO_2-hydrate in a porous medium. The model included the influences of pore walls and other possible complications on nucleation. They recovered a surface tension, 0.0015 J/m^2, which was about 18 times smaller than the surface tension between ice and water. This value implied that the effective surface energy of the nuclei was smaller than that predicted from homogenous nucleation, and was consistent with the expectations they had that the pore walls and other foreign particles served as nucleation sites and promote nucleation. [32] There is a possibility that the assumed surface tension in the present study should be determined in the same manner that Zatsepina and Buffett did, in order to get more accurate results for the radius of critical size water clusters.

3.9: The Cell constant.

The cell properties were assumed to have an impact on energy barrier and activation energy, as it was observed that experiments conducted in different cells with the same type of fluid gave different energy barrier at similar experimental conditions. This could be due to a "cell constant" affecting the nucleation process inside the cell. If quantified such cell constant could enhance the knowledge of the "unaffected" activation energy.

If we introduce a cell constant E_c, that serves as the part of the activation energy and is due to the cell system itself, we could probably assume a relation for the total energy barrier (Gibbs free energy difference, ΔG) to be:

$$\Delta G = E_c + E_a \qquad (3.9.1)$$

Where ΔG is the change in Gibbs free energy (energy barrier, often referred to as an activation energy) calculated from the Arrhenius equation, E_c is the contribution of activation energy coming from the cell, and E_a is the contribution of activation energy coming from the chemical composition (liquid and gas).
The change in activation energy that we see from the comparison between two experimental series with identical experimental properties conducted in different cells can be said to be purely a change in the cell constants between the two cells, as the contribution of activation energy coming from the chemical composition is assumed to be unchanged if the liquid and gas properties are kept constant. This difference in the cell constants can be written as:

$$\Delta G_1 - \Delta G_2 = \left(E_{c,1} + E_a\right) - \left(E_{c,2} + E_a\right) \qquad (3.9.2)$$

and

$$\Delta G_1 - \Delta G_2 = E_{c,1} - E_{c,2} = \Delta E_c \qquad (3.9.3)$$

Where ΔG_1 and ΔG_2 are the activation energy calculated from the Arrhenius equation for experimental series 1 and 2 conducted in different cells, $E_{c,1}$ and $E_{c,2}$ are the estimated complications on nucleation affecting the activation energy measured from the experimental series 1 and 2 conducted in different cells, while E_a is the contribution to the activation energy in an "undisturbed" process. ΔE_c in equation (3.9.3) represents the difference in the

contribution of activation energy due to possible complications to nucleation caused by the cells between experimental series 1 and 2.

3.10: Analysis of data.

Analytical tools used:

- LabView: logging program by National Instruments that monitors the temperature in the gas and liquid phase, the pressure response in the cells, and time. The logging frequency was set to every fifth second
- KaleidaGraph: by Synergy Software that was mainly used to find induction times for the experiments
- CSMGem: by Colorado School of Mines that was used to calculate the equilibrium temperature for SNG-7/methane at experimental pressure. Note that the equilibrium temperature calculated from this program may deviate from the reality, because no program available can perform this accurately. The equilibrium temperature calculated from CSMGem is approx. 0.1-0.2 ^{o}C lower than it would be in reality. The previous generation CSMHyd calculates a little lower equilibrium temperature compared to CSMGem, but as CSMGem serves as an improvement over the previous generation the equilibrium temperatures were taken from this program
- MatLab: used to find the nucleation rates and lag times for the different experimental temperatures involved in an experimental series

Graphical analysis of experimental data in KaleidaGraph:

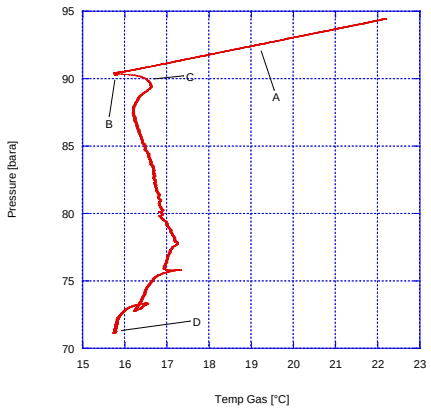

- **Graph 3.10.1: A typical graph of the logged data in LabView (reconstructed here in KaleidaGraph). A) The PT-curve follows a linear relation during cooling, B) Hydrate is formed, which is an exothermic reaction. Pressure decreases as a result of gas consumption, C) The temperature stops increasing, and D) The gas consumption ends, indicating that the hydrate has stopped growing**

From the experimental data one can see that the PT-curve follows a linear relation during the cooldown. It is therefore possible to perform a linear regression analysis which gives the relation between the pressure in the system without hydrate formed and the temperature. This was done to determine which starting pressure at the starting temperature that had to be used in the experiments in order to reach the experimental pressure and temperature keeping the same cooling rate used for the other experiments. This linear relation was similar in all experiments. The relation is shown below:

$$P = 83{,}789 + 0{,}68598T \qquad (3.10.1)$$

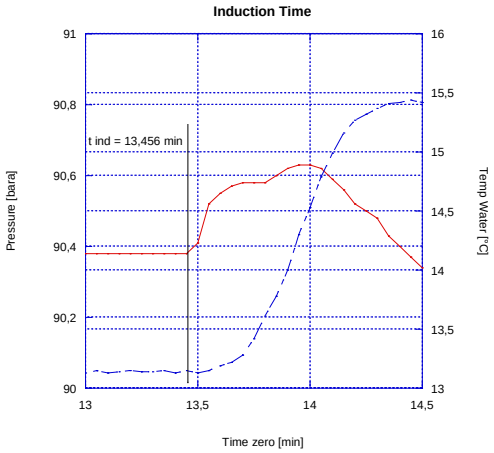

- **Graph 3.10.2: Graph showing induction time determined from the pressure and temperature response in one of the experiments conducted in this thesis. Time from start of experiments to onset of hydrate formation, t_ind (induction time) = 13.456 min**

The way the induction times were determined for all experiments is shown in the above figure. A small pressure jump (which was visible in all experiments) was taken as the point of hydrate formation. Induction time was therefore set here. This pressure jump found place before the temperature response to hydrate formation in both liquid and gas.

Induction times have only been used to determine the nucleation rates and lag times for the experimental series conducted in the present study.

They were ranged from the lowest to the highest induction time. The lowest is taken as the least probable duration of time to get hydrate formation, whereas the highest induction time is assumed to be the duration of time from start of experiments when one is 100 % sure that hydrate has been formed in the cells.

4. **Results and discussion.**

4.1: Nucleation rates and lag times.

The induction times measured during parallel experiments were fitted to the nucleation probability distribution function shown in section 3.7. MatLab was used to estimate the nucleation rates and lag times from the theoretical distribution function with the experimental distribution data as input. Lag times were not used for any analysis in this thesis, but they are presented here to give an idea on the time interval between the appearance of a stable cluster and its experimental detection. Negative lag times means that there is a probability that the nucleation process could commence during the cooling section prior to start of stirring.

Measured nucleation rates and lag times are shown in Table 4.1.1 below.

- **Table 4.1.1: Nucleation rates and lag times for all experiments. DW stands for distilled water. Experimental properties are included**

Cell nr.	Inhibitor	Cooling rate [°C/h]	RPM	P_{exp} [bar]	T_{exp} [°C]	J [min^{-1}]	τ_0 [min]
1	DW	6,75	619	90	13	0,456600	-0,301800
					14,25	0,007526	-34,83000
					15,5	0,005838	214,20000
	DW	6	710	61	10	0,054220	-6,525000
					10,5	0,052270	-5,775000
					11	0,020240	-10,89000
	50 ppm PVCap	6	710	61	10	0,422700	-0,094040
					10,5	0,087600	-4,40900
					11	0,005262	-25,05000
2*	DW	3	425	90	6	0,316100	-0,47430
					7	0,066840	-2,36500
					8	0,011860	-12,45000
3	DW	6	619	61	11	0,070960	-1,75900
					12	0,025290	-9,74300
					13	0,010010	-16,80000
	50 ppm PVP	6	619	61	11	0,820800	-24,62000
					12	0,023260	48,16000
					13	0,010830	-5,23900
	DW	6,75	619	90	13	0,108000	0,98110
					14,25	0,013680	-26,78000
					15,5	0,005045	-6,79000
	50 ppm PVCap	6,75	619	90	13	0,036840	27,12000
					14,25	0,033320	43,09000
					15,5	0,008774	-17,08000
	DW	2	619	90	13	0,165800	-2,36100
					14,25	0,075710	5,20000
					15,5	0,006653	-26,99000

- ***: All experiments in Cell #2 are conducted on pure, scientific grade methane. All experiments in Cell #1 and #3 are on SNG-7**

4.2. Activation energy.

The natural logarithm of the nucleation rates was plotted as function of the inverse of the experimental temperatures for each series in order to determine the activation energy of the individual series. This was done following the method explained in section 3.8. The activation energy and radius of critical cluster for each experimental series is shown in the below table.

- **Table 4.2.1: Calculated activation energy, ΔG_{crit}, and radius of the critical size water cluster, r_{crit}, for every experimental series**

Cell nr.	Inhibitor	Cooling rate [°C/h]	RPM	P_{exp} [bar]	ΔG_{crit} *10^{18} [J]	r_{crit} [Å]
3	DW	6	619	61	1,10	30,84
	DW	6,75	619	90	1,40	34,78
	DW	2	619	90	1,47	35,61
	50 ppm PVP	6	619	61	2,43	45,86
	50 ppm PVCap	6,75	619	90	0,654	23,78
2	DW	3	425	90	1,78	39,22
1	DW	6	710	61	1,09	30,76
	DW	6,75	619	90	1,99	41,50
	50 ppm PVCap	6	710	61	4,87	64,91

The baseline experiments on pure water in Cell #3 indicates that the energy barrier and the critical cluster size radius increases with increasing pressure in the region between 61 and 90 bar (27.3 % and 12.8 % respectively). Apparently the energy barrier and critical size cluster radius increases with decreasing cooling rate from 6.75 to 2 °C/h (5 % and 2.4 % respectively). The former increase can probably be regarded significant, while the

significance of the latter increase is most probably too small within the accuracy of the method.

Cell #3 experiments at 61 bar showed that 50 ppm PVP increased the energy barrier by factor 2.2 as compared to the baseline condition. PVP could probably affect the surface tension between water and the hydrate. Mark Rodger conducted molecular dynamic simulations (MD) on PVP systems and found that PVP disturbs the water structure and moves away from the hydrate surface when hydrate form without being bound or attached to the surface. Thus it could be assumed that effect on the surface tension at the water – hydrate interface may be negligible. Based on the surface tension at a water – hydrate interface 50 ppm PVP gave increased critical radius from 30.84 Å (baseline) to 45.86 Å (48.7 %).

Cell #3 experiments at 61 bar showed that 50 ppm PVCap reduced the energy barrier by factor 1.7 as compared to the baseline condition. MD simulations by Mark Rodger's group at the University of Warwick, UK has shown that PVCap have a tendency to structure water in a hydrate-like structure around the Cap monomer units and that the Cap units will be adsorbed or bound to the hydrate surface when hydrates form. [36] Thus it is reasonable to assume that the surface tension at the water – hydrate surface will be affected and that calculations of critical radius with the surface tension at the water – ice interface most probably is incorrect. However, the estimated critical radius of 23.78 Å with 50 ppm PVCap present shows that PVCap is promoter for hydrate nucleation. The PVCap promoter effect is in agreement with previous work by Abay et al. [44]

4.3: Activation energy – Comparison.

The previous section presented the activation energy and radius of the critical size water cluster for every experimental series in this thesis. A comparison of these results has been made in order to achieve a better understanding of the activation energy concept.

It was reasoned that only the type of fluid involved in the experiments had any impact on the value of activation energy for pure systems without KHI present.

The experimental series conducted in Cell #2 was not compared to any other series, because this series was conducted on pure methane gas without supplementary experiments on KHI systems.

4.3.1: DW vs. 50 ppm PVCap 61 bar in Cell #1.

The activation energy in the experimental series with PVCap was higher as compared to the activation energy in baseline system with pure, distilled water.
According to theory, the activation energy for the PVCap series should be lower than the activation energy for the distilled water series. This is due to PVCap being a promoter of the nucleation phase. Too few experiments conducted for these experimental series or mechanical equipment problems can be an explanation on why we don`t see a lower activation energy in the PVCap series. It has been observed through other student works in the lab that Cell #1 responds differently from the other similar three cells. It has been observed that it is more difficult to nucleate hydrates in Cell #1 at pressures above 60 bars and that lower temperatures or longer time is required for hydrates to nucleate. [7] Cell #1 experiments are therefore regarded more uncertain as compared to Cell #3 and Cell #2 experiments.

4.3.2: DW vs. 50 ppm PVP 61 bar in Cell #3.

The experimental results showed that the activation energy during experiments with PVP was higher as compared to the activation energy in the baseline, distilled water system.
The increase in activation energy with PVP in the system is according to MD simulations by Mark Rodger's group [36]. The KHI PVP disturbs water structure and acts as an inhibitor on the nucleation phase, which means that the energy barrier most probably is increased for the PVP system as compared with the baseline.

4.3.3: DW vs. 50 ppm PVCap 90 bar in Cell #3.

The activation energy in the experimental series with PVCap was lower compared to the activation energy for the experimental series with distilled water.

Lower activation energy in the PVCap series compared to the baseline is assumed reasonable since PVCap can act as hydrate promoter at low concentrations as discussed above.

4.3.4: DW 90 bar vs. 61 bar in Cell #3.

The DW baseline at 90 bar (6.75 ^{o}C/h) was compared to the DW baseline at 61 bar (6 ^{o}C/h). These experiments were conducted at different conditions with respect to pressure and temperature, and the comparison was made in order to examine whether the energy barrier was function of fluid system only or if pressure would have significant effects. The series are plotted together in the graph below:

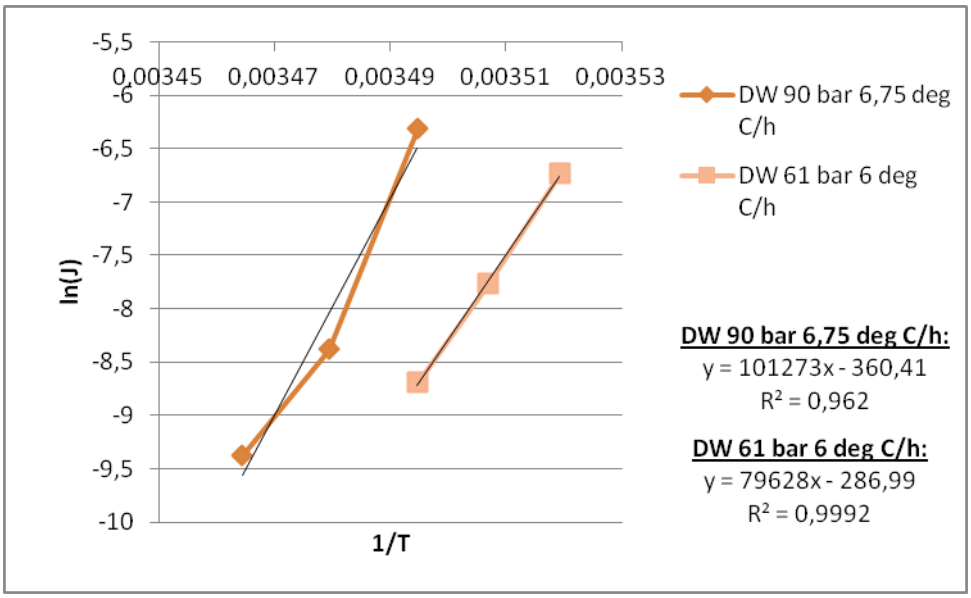

- **Graph 4.3.4.1: Arrhenius plot of the DW series at 90 bar (6.75^{o}C/h) vs. the DW series at 61 bar (6 ^{o}C/h) in Cell #3**

The activation energies in these series were comparable within approx. 27 %, with highest energy barrier at the highest pressure. The difference in critical water cluster size was 12.8 %. However, it should be noted that there is a change in the pre-exponential factor J_0 as can be seen from graph 4.3.4.1. The pre-exponential factor expresses a “steady state” nucleation rate of the system and for nucleation from water this rate is obtained at hydrate equilibrium at given pressure.

4.3.5: Cooling rate 6.75 °C/h vs. 2 °C/h at 90 bar, DW and in Cell #3.

Both experimental series had the exact same experimental conditions except for the cooling rate.

The reason for doing this comparison is to see if a reduced cooling rate would have any impact on the activation energy. As it was written in section 2.8 for the experiments done with SNG-7, a reduced cooling rate results in increased nucleation rates compared to the same system with a higher cooling rate. This statement was confirmed from the experiments conducted in the two experimental series in question. According to this, one can then expect an increase in activation energy for the series with cooling rate of 2 °C/h compared to the series with cooling rate of 6.75 °C/h, as an increase in nucleation rates results in an increase in activation energy.

The activation energy increase by approx. 5% by reducing the cooling rate from 6.75 °C/h to 2 °C/h. It was also observed that the reduction in cooling rate did not significantly change the pre-exponential factor J_0 as shown in graph 4.3.5.1 below.

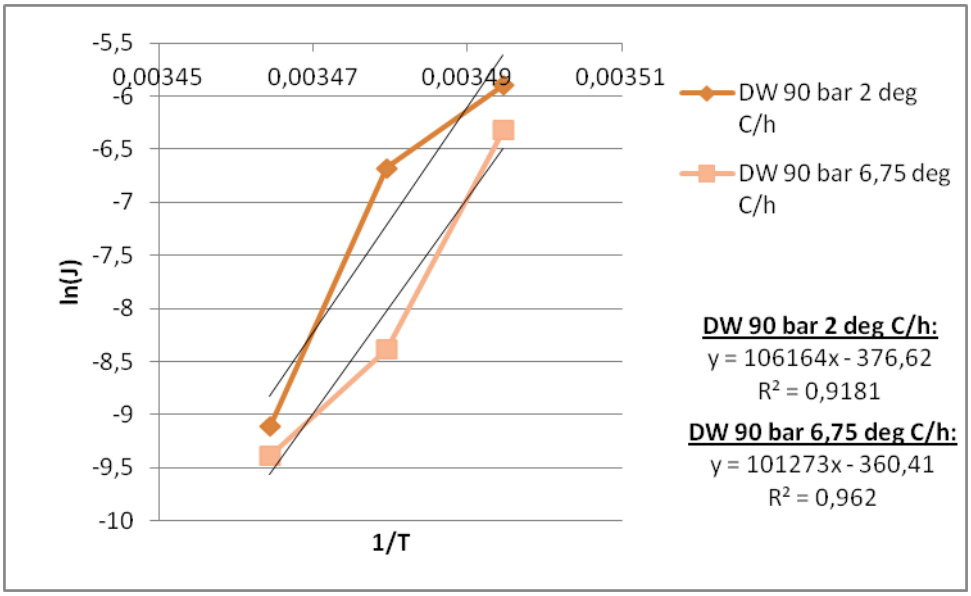

- **Graph 4.3.5.1: Arrhenius plot of the DW series with a cooling rate of 2 °C/h vs. the DW series with a cooling rate of 6.75 °C/h. Both series were performed at 90 bar in Cell #3**

4.3.6: DW 90 bar vs. 61 bar in Cell #1.

The DW baseline at 90 bar (6.75 ^{o}C/h) was compared to the DW baseline at 61 bar (6 ^{o}C/h). These experiments were conducted at different conditions with respect to pressure and temperature, and the comparison was made in order to examine whether the energy barrier was function of fluid system only or if pressure would have significant effects. The series are plotted together in the graph below:

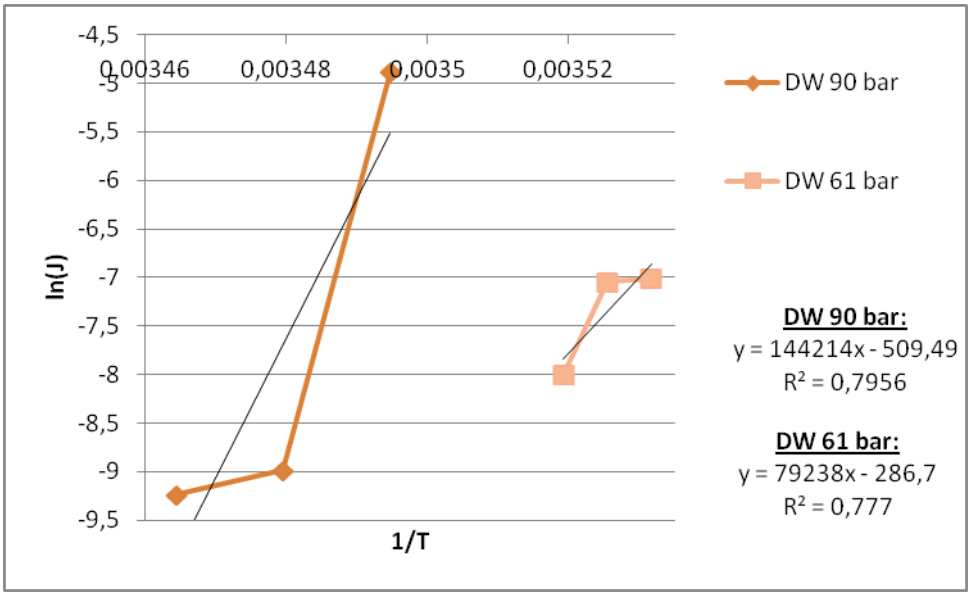

- **Graph 4.3.6.1: Arrhenius plot of DW 90 bar vs. 61 bar in Cell #1**

The activation energies in these series were comparable within approx. 83 %, with the highest energy barrier at the highest pressure. The difference in critical water cluster size was 35 %. It was also observed a change in the pre-exponential factor.

One can see from graph 4.3.6.1 that the R^2 values for the DW 61 bar series and DW 90 bar series are relatively low, indicating that the data points for the experimental series deviate significantly from a straight line. The reason for this deviation could be that too few experiments have been performed for the experimental series. There are also problems with Cell #1, as was discussed earlier in this thesis. Cell #1 has a cell response that may not suit this kind of experiments.

On basis of the low R^2 values and problems with experiments in Cell #1, the result from the comparison between DW 90 bar and DW 61 bar is not reliable.

4.3.7: DW in Cell #3 vs. DW in Cell #1 at 90 bar and 6.75 ^{o}C/h.

Experiments on SNG-7 hydrate nucleation from distilled water at 90 bars and 6.75 ^{o}C/h were conducted both in Cell #3 and Cell #1 at exact same experimental conditions to examine and compare the performances of the cells. The reason for doing this comparison is to try and quantify the differences caused by the cells themselves.

The results show that the activation energy measured in these cells at similar conditions is not exactly the same. This supports an assumption that the cell properties affect the measured and apparent activation energy. The differences in measured activation energy and critical size water cluster radius were approx. 42 % and approx. 19 % respectively.

4.3.8: DW 90 bar Cell #2: Determination of Cell constant.

If we assume the estimated radius of critical size water cluster made by Larson and Garside to be free of cell effects, this can be used to determine the cell constant for the experimental Cell #2 used in the present study.

The radius suggested by Larson and Garside was stated to be 32 Å in section 2.6. By implementing equation (3.8.7), we get the activation energy related to this radius to be $1.18*10^{-18}$ J. This activation energy corresponds to E_a in equation (3.9.1).

The activation energy from the DW series at 90 bar conducted in Cell #2 was $1.78*10^{-18}$ J. It is assumed that the cell effects have an impact on this activation energy.

Equation (3.9.2) can then be used to give an estimate of the cell constant for Cell #2 with basis on the above values of activation energy. This is done by subtracting the activation energy calculated from the estimated radius made by Larson and Garside with the calculated activation energy from the DW series at 90 bars in Cell #2. The result is an estimate for the cell constant: $E_{Cell\#2} = 6*10^{-19}$ J. The cell constant increases the activation energy by approx. 50 % compared to the "unaffected" activation energy of the system. The positive value of the cell constant may be an indication of the cell having a negative effect on nucleation, increasing the energy needed to achieve a critical size water nucleus. The cell constant therefore provides activation energy higher than the real activation energy of the system.

4.3.9: DW 90 bar Cell #2: Nucleation vs. self-sustaining growth.

Determination of the activation energy needed to obtain a self-sustaining macroscopic growth has been the focus of many papers on hydrate research. However, their means of obtaining the critical radius related to this activation energy seems a little unclear. It seems impossible to find this radius using the classical nucleation theory, when not knowing the activation energy for the formation of a critical size water cluster. So, in this section, another idea is presented on how to calculate the critical nucleus radius needed for a self-sustaining macroscopic growth.

This idea is based on the classical nucleation theory and assuming that we know both the activation energy needed to form a critical size water cluster, ΔG_{crit}, and the activation energy needed to obtain a self-sustaining macroscopic growth, ΔG_{growth}.

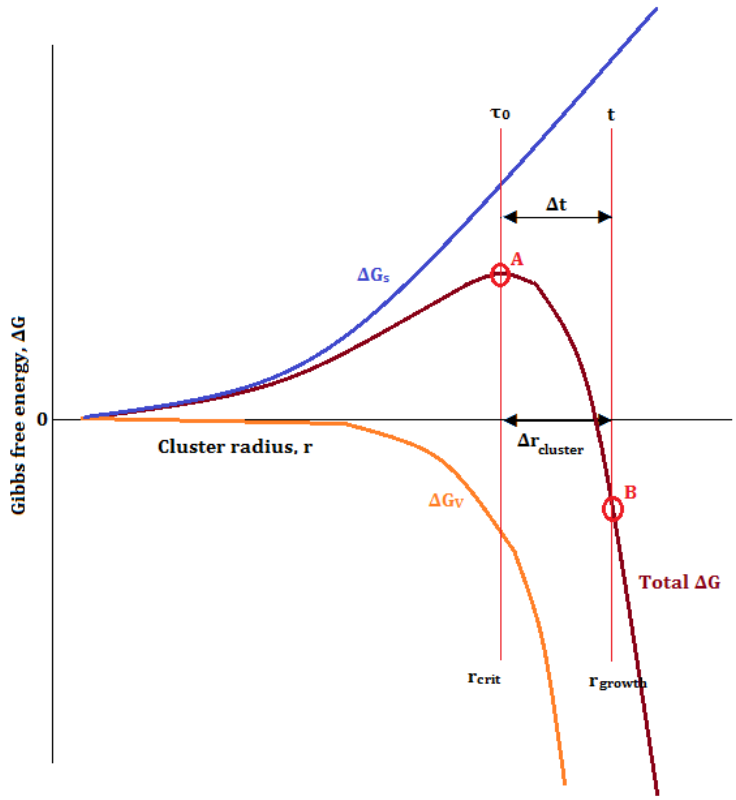

- **Graph 4.3.9.1: A graphical illustration of Gibbs free energy as a function of cluster radius. Two important points in this graph are point A which shows the activation energy needed to form critical size water cluster (which is the focus of this thesis) and point B which represents the activation energy needed in order to obtain a critical size nucleus for the macroscopic growth process to proceed self-sustainingly. NB: τ_0 in this graph is not lag time, but the time of appearance of a cluster. Also, t is the time until a self-sustaining macroscopic growth is achieved (modified from figure 2.6.2)**

The radius of a critical size water cluster can easily be calculated from its activation energy using the classical nucleation theory. This however, cannot be done with ΔG_{growth} as this is a negative value. Referring to equation (3.8.8), one can see that a negative value gives no answer for the radius of the critical size nucleus needed for a self-sustaining macroscopic growth due to the square root in the function.

However, if we take the energy difference between ΔG_{growth} and ΔG_{crit}, we get the additional amount of energy needed to go from a critical size water cluster to a critical size nucleus. This additional energy reflects how much the radius of the critical size water cluster has to increase in order to become a critical size nucleus. Adding this energy difference to ΔG_{crit}, we get the total activation energy (including ΔG_{crit}) for the self-sustaining macroscopic growth, ΔG_{tot}. By inserting the value of ΔG_{tot} in equation (3.8.8), we can calculate the radius, r_{growth}, related to ΔG_{growth}.

As an example on the use of this idea with real values of activation energy, we will look at the radius of a critical size methane nucleus.

We first take the activation energy for the critical size water cluster from the distilled water series conducted in Cell #2, and the activation energy for the critical size nucleus calculated by Bergeron et al. as mentioned in section 3.8. These are 1071 kJ/mol and -323 kJ/mol respectively, and both are related to methane system. The energy difference is 1394 kJ/mol.

The calculated radius of the critical size water cluster for the distilled water series conducted in Cell #2 was 39.22 Å, while Larson and Garside estimated the cluster size to be 32 Å from nucleation theory as was stated in section 2.6.

By multiplying the energy difference of 1394 kJ/mol with 1000 and dividing it with Avogadros number ($6.0221415*10^{23}$ mol^{-1}), we get the energy difference in unit Joule: $2.31*10^{-18}$J. Inserting this value into equation (3.8.8), we get the additional radius 44.7 Å. This additional radius plus the radius of the critical size water cluster (39.22 Å), gives us r_{growth} = 83.92 Å. This result is in agreement with the size range of 30-170 Å calculated by Englezos et al. and the proposed methane critical nucleus radius of approx. 100 Å made by Nerheim et al. as was written in section 2.6.

There have been no experiments conducted on calculating the radius of the critical size water cluster and the radius of the critical size nucleus for the SNG-7 gas used in the other experiments in the present study. But as SNG-7 contains 80.4 mol% methane, one can draw the assumption that the estimated critical size water cluster radius of 32 Å made by Larson and Garside and the size range 30-170 Å for radius of critical size nucleus calculated by Englezos et al. and the proposed radius of critical size nucleus of approx. 100 Å made by Nerheim et al. also is valid for this type of gas.

5. **Conclusion.**

The Arrhenius equation can be applied to calculate the activation energy for the formation of a critical size water cluster.

By assuming heterogeneous nucleation, and the surface tension between hydrate and water to be 0.0276 J/m^2, one can calculate the radius of the critical size water cluster related to this activation energy.

The critical nucleus radius for methane system calculated from the idea presented in the end of chapter 4 corresponds to the size range determined by Englezos et al. and the proposed critical nucleus radius by Nerheim et al. The radius of critical size water cluster calculated for the distilled water series conducted in Cell #2 with pure methane was similar to the estimated critical size water cluster made by Larson and Garside. One can draw the assumption that this also is valid for the experimental series with SNG-7, when considering that SNG-7 contains 80.4 mol% methane.

The activation energy was shown to mainly be dependent on type of fluid in the system in pure systems without KHI present, as experimental series conducted in the same cell with different experimental conditions but with the same type of liquid and gas gave similar activation energy.

An increase of activation energy of approx. 27 % by increasing the pressure from 61 to 90 bars was observed, but the number of pressures (2) are too few to make a final conclusion on effect of pressure.

It was also concluded that the experimental cells could have an impact on the activation energy, as experiments conducted in Cell #1 and Cell #3 with exact same experimental conditions gave different activation energies. This could be due to problems of mechanical character in Cell #1, but this has not been verified by repeating the experiments in one of the other, similar cells (Cell #0 or Cell #2, occupied by other students). Apparently Cell #1 required higher driving force for nucleation to occur and behaved more “stochastic” than the other cells. The results from Cell #1 are thus assumed less reliable than Cell #3 (SNG-7 system) and Cell #2 (pure methane) experiments.

In Cell #3 PVCap gave an activation energy lower than distilled water baseline. This result is logical because PVCap could act as a promoter on the nucleation process. PVCap may cause water molecules to arrange in a hydrate like structure around the Cap monomer heads. On the other hand, in Cell #1 PVCap gave activation energy higher than distilled water baseline. An explanation for the deviating Cell #1 behavior could be due to mechanical equipment problems or too few experiments performed resulting in overestimated activation energy.

PVP (Cell #3) gave activation energy higher than the distilled water baseline. The explanation for this is that PVP disturbs water structure and acts as an inhibitor on the nucleation phase.

A slight increase of activation energy by approx. 5 % was observed in Cell #3 at 90 bars reducing cooling rate from 6.75 °C/h to 2 °C/h, but the number of cooling rates examined (2) are too few to make final conclusion on effect of cooling.

For future work, it is recommended to accurately determine the surface tension between hydrate and water in the system as the value for this was only assumed in the present study. The value of the surface tension between hydrate and water is of great importance when calculating the critical radius of the cluster. The surface tension may be influenced by experimental equipment (cell wall) or foreign particles (dust) which serve as nucleation sites and promote nucleation. It may also be affected by other factors such as the addition of kinetic inhibitors (PVCap, PVP). The surface tension between hydrate and water should therefore be determined by either direct measurement or from a model which incorporates all effects and factors influencing the surface tension. This may result in improved values closer to reality for the radius of critical sized water clusters.

It would also be recommended to look into the effect the volumes of fluid (liquid and gas) has on the value of activation energy, as this effect was not addressed in this thesis.

6. References.

1. Sloan, E.D. and C.A. Koh, *Clathrate hydrates of natural gases*. 2008, CRC Press: Boca Raton, Fla. p. 1-29.
2. Yuri F, M., *Natural gas hydrates – A promising source of energy*. Journal of Natural Gas Science and Engineering, 2010. **2**(1): p. 49-59.
3. Sloan, E.D. and C.A. Koh, *Clathrate hydrates of natural gases*. 2008, CRC Press: Boca Raton, Fla. p. 634-679.
4. Wu, M., S. Wang, and H. Liu, *A Study on Inhibitors for the Prevention of Hydrate Formation in Gas Transmission Pipeline.* Journal of Natural Gas Chemistry, 2007. **16**(1): p. 82.
5. Kelland, M.A., *History of the development of low dosage hydrate inhibitors.* Energy and Fuels, 2006. **20**(3): p. 825-847.
6. Sloan, E.D. and J.B. Bloys, *Hydrate engineering*. Monograph. Vol. 21. 2000, New York: SPE. p. 89.
7. Svartaas, T.M., *Personal communication*, 2012.
8. Hammerschmidt, E.G., *Formation of Gas Hydrates in Natural Gas Transmission Lines.* Industrial & Engineering Chemistry, 1934. **26**(8): p. 851-855.
9. Sloan, E.D., C.A. Koh, and A.K. Sum, *Natural Gas Hydrates in Flow Assurance*. 2011, Gulf Professional Pub./Elsevier: Burlington, MA. p. 1-11.
10. Sloan, E.D., C.A. Koh, and A.K. Sum, *Natural Gas Hydrates in Flow Assurance*. 2011, Gulf Professional Pub./Elsevier: Burlington, MA. p. 13-36.
11. Carroll, J.J., *Natural gas hydrates: a guide for engineers*. 2003, Gulf Professional Publ.: Amsterdam ; Boston. p. 165-197.
12. Bergeron, S., J.G. Beltrán, and P. Servio, *Reaction rate constant of methane clathrate formation.* Fuel, 2010. **89**(2): p. 294-301.
13. Vysniauskas, A. and P.R. Bishnoi, *A kinetic study of methane hydrate formation.* Chemical Engineering Science, 1983. **38**(7): p. 1061-1972.
14. Vysniauskas, A. and P.R. Bishnoi, *Kinetics of ethane hydrate formation.* Chemical Engineering Science, 1985. **40**(2): p. 299-303.
15. Jeffrey, G.A., *Inclusion Compounds*, ed. J.L. Atwood, J.E.D. Davies, and D.D. MacNichol. 1984: Academic Press. p. 135.
16. Sloan, E.D. and C.A. Koh, *Clathrate hydrates of natural gases*. 2008, CRC Press: Boca Raton, Fla. p. 45-102.

17. Lyusternik, L.A., *Convex Figures and Polyhedra*. 1963, New York: Dover.
18. Carroll, J.J., *Natural gas hydrates: a guide for engineers*. 2003, Gulf Professional Publ.: Amsterdam ; Boston. p. 17-49.
19. Høvring, E., *Effect of PVCap-6K in concentrations of 50, 100, 500, 1000, 2000, 3000 and 5000 ppm on nucleationrate and crystalgrowth for structure II SNG-7 (Synthetic Natural Gas 7 Component) hydrate*, in *Petroleum technological institute*2010, University in Stavanger: Stavanger. p. 58.
20. Lekvam, K., *Kinetics of natural gas hydrates*, 1995, HIS: Stavanger. p. 42-43.
21. Svartås, T.M. and L.A. Dybvik, *Studies of Novel Hydrate Inhibitors Part 2 - Kinetic Effects and Mechanisms*, 1993, Esso Norge AS: Stavanger. p. 4-5.
22. Svartås, T.M. and L.A. Dybvik, *Studies of Novel Hydrate Inhibitors Part 2 - Kinetic Effects and Mechanisms*, 1994, Esso Norge AS: Stavanger. p. 5-6.
23. Sloan, E.D. and C.A. Koh, *Clathrate hydrates of natural gases*. 2008, CRC Press: Boca Raton, Fla. p. 113-181.
24. Wyslouzil, B.E., J.L. Cheung, G. Wilemski, and R. Strey, *Small angle neutron scattering from nanodroplet aerosols.* Physical Review Letters, 1997. **79**(3): p. 431-434.
25. Volmer, M. and A. Weber, *Keimbildung in übersättigten Gebilden.* Z. Phys. Chem. (Leipzig), 1926. **119**: p. 277-301.
26. Smith, J.M., H.C. Van Ness, and M.M. Abbott, *Introduction to chemical engineering thermodynamics*. 2005, McGraw-Hill. p. 199-230.
27. Nerheim, A.R. and T.M. Svartaas. *Investigation of hydrate kinetics in the nucleation and early growth phase by laser light scattering*. in *Proceedings of the Second International Offshore and Polar Engineering Conference*. 1992. San Francisco: The International Society of Offshore and Polar Engineers.
28. Larson, M.A. and J. Garside, *Solute clustering in supersaturated solutions.* Chemical Engineering Science, 1986. **41**(5): p. 1285-1289.
29. Vehkamäki, H., *Classical Nucleation Theory in Multicomponent Systems*. 2006, Springer-Verlag Berlin Heidelberg. p. 135-151.
30. Arjmandi, M., B. Tohidi, A. Danesh, and A.C. Todd, *Is subcooling the right driving force for testing low-dosage hydrate inhibitors?* Chemical Engineering Science, 2005. **60**(5): p. 1313-1321.

31. Radhakrishnan, R. and B.L. Trout, *A new approach for studying nucleation phenomena using molecular simulations: Application to CO[sub 2] hydrate clathrates.* The Journal of Chemical Physics, 2002. **117**(4): p. 1786-1796.
32. Zatsepina, O.Y. and B.A. Buffett, *Nucleation of CO2-hydrate in a porous medium.* Fluid Phase Equilibria, 2002. **200**(2): p. 263-275.
33. Kelland, M.A., T.M. Svartaas, J. Øvsthus, T. Tomita, and J.-i. Chosa, *Studies on some zwitterionic surfactant gas hydrate anti-agglomerants.* Chemical Engineering Science, 2006. **61**(12): p. 4048-4059.
34. Abay, H.K. and T.M. Svartaas, *Multicomponent Gas Hydrate Nucleation: The Effect of the Cooling Rate and Composition.* Energy & Fuels, 2010. **25**(1): p. 42-51.
35. Kvamme, B., T. Kuznetsova, and K. Aasoldsen, *Molecular dynamics simulations for selection of kinetic hydrate inhibitors.* Journal of Molecular Graphics and Modelling, 2005. **23**(6): p. 524-536.
36. Rodger, P.M. *Hydrate Nucleation and Inhibition: New Methods for Deeper Understanding*. in *Proceedings of the 7th International Conference on Gas Hydrates (ICGH 2011)*. 2011. Edinburgh, Scotland, UK.
37. Abay, H.K. and T.M. Svartaas, *Effect of Ultralow Concentration of Methanol on Methane Hydrate Formation.* Energy & Fuels, 2009. **24**(2): p. 752-757.
38. Toschev, S., A. Milchev, and S. Stoyanov, *On some probabilistic aspects of the nucleation process.* Journal of Crystal Growth, 1972. **13–14**(0): p. 123-127.
39. Milchev, A., *Electrocrystallization: fundamentals of nucleation and growth*. 2002, Boston, Mass.: Kluwer Academic. p. 165.
40. Jiang, S. and J.H. ter Horst, *Crystal Nucleation Rates from Probability Distributions of Induction Times.* Crystal Growth & Design, 2010. **11**(1): p. 256-261.
41. Abay, H.K., *Kinetics of gas hydrate nucleation and growth*, 2011, UiS: Stavanger.
42. Rodríguez-Díaz, J.M. and M.T. Santos-Martín, *Study of the best designs for modifications of the Arrhenius equation.* Chemometrics and Intelligent Laboratory Systems, 2009. **95**(2): p. 199-208.
43. Arrhenius, S., *Ober die reacktionsgeschwindigkeit bei der inversion von rohrzucker durch saüren.* Z. Physik. Chem, 1889. **4**: p. 226-248.
44. Abay, H.K., E. Hovring, and T.M. Svartas. *Does PVCap Promote Nucleation Of Structure II Hydrate?* in *Proceedings of the 7th International Conference on Gas Hydrates (ICGH 2011)*. 2011. Edinburgh, Scotland, UK.

7. Appendix.

- **Table 7.1: List of experimental performers and number of experiments in every experimental series**

Cell nr.	No. Expr	Performer
1	18	Eirik Høvring
	45	Leif Inge Kjærvoll
2	22	Magnus Palm
3	36	Silje Bru
	64	Eirik Høvring